



**HAL**  
open science

## Enhanced 3D solid finite element formulation for rotor dynamics simulation

Zihan Shen, Benjamin Chouvion, Fabrice Thouverez, Aline Beley

► **To cite this version:**

Zihan Shen, Benjamin Chouvion, Fabrice Thouverez, Aline Beley. Enhanced 3D solid finite element formulation for rotor dynamics simulation. *Finite Elements in Analysis and Design*, 2021, 195, pp.103584. 10.1016/j.finel.2021.103584 . hal-03390409

**HAL Id: hal-03390409**

**<https://hal.science/hal-03390409>**

Submitted on 13 Jun 2023

**HAL** is a multi-disciplinary open access archive for the deposit and dissemination of scientific research documents, whether they are published or not. The documents may come from teaching and research institutions in France or abroad, or from public or private research centers.

L'archive ouverte pluridisciplinaire **HAL**, est destinée au dépôt et à la diffusion de documents scientifiques de niveau recherche, publiés ou non, émanant des établissements d'enseignement et de recherche français ou étrangers, des laboratoires publics ou privés.



Distributed under a Creative Commons Attribution - NonCommercial 4.0 International License

# Enhanced 3D solid finite element formulation for rotor dynamics simulation

Zihan Shen<sup>a,b,\*</sup>, Benjamin Chouvion<sup>a,c</sup>, Fabrice Thouverez<sup>a</sup>, Aline Beley<sup>b</sup>

<sup>a</sup>*Ecole Centrale de Lyon, LTDS, CNRS UMR 5513, 69130 Ecully, France*

<sup>b</sup>*ANSYS-France, 69100 Villeurbanne, France*

<sup>c</sup>*Centre de recherche de l'Ecole de l'air, 13300 Salon-de-Provence, France*

---

## Abstract

In this paper, an enhanced solid finite element formulation for rotor dynamics analysis is presented. The element kinematics is first defined with a Total Lagrangian formulation in order to account for possible centrifugal stiffening effect and its associated pre-stress deformation. The novelty of the three-dimensional element proposed in this study is then to correctly consider the effect of inertia due to small rotational deformation occurring around the pre-stressed equilibrium position. The rotational motion is characterized by interpolation of the translational degrees of freedom of the element. The accuracy and convergence of the proposed finite element are tested on several numerical examples consisting of a rotating rigid disk and a rotating Timoshenko beam with different slenderness ratios. All results agree well with analytical solutions excerpted from literature and demonstrate the usefulness and applicability of the proposed finite element formulation.

---

\*Corresponding author.

*Email address:* [zihan.shen@doctorant.ec-lyon.fr](mailto:zihan.shen@doctorant.ec-lyon.fr) (Zihan Shen)

*Keywords:* rotor dynamics; finite element formulation; spin-softening;  
centrifugal-stiffening

---

## 1 **1. Introduction**

2 Performing a direct association between three-dimensional (3D) designs  
3 and finite element (FE) simulations is current practice in many engineering  
4 applications to shorten the development cycle time. In rotating machines,  
5 as the design of rotors is developed via 3D software to accurately define for  
6 instance advanced geometrically complex blades, the utilization of 3D solid  
7 FE modeling is inevitable for a good prediction of the dynamics behavior. 3D  
8 solid FEs have been widely employed to investigate the dynamic responses  
9 to various rotating structures, such as rotating beam-like structures [1, 2],  
10 rotating annular plates [3], and rotating cylinders [4].

11 When the rotor is considered as a rigid body, the definition of the ro-  
12 tational motion is clear. If a general flexible structure is tackled, the de-  
13 formation parameter and the angular velocity vary simultaneously from a  
14 material point to another within the rotating body. Without rotational de-  
15 grees of freedom, one cannot correctly define this rotation at each particle  
16 contained in the continuous structure. Thus, it is not straightforward to  
17 characterize exactly what the spin speed of the rotor is within the solid FE  
18 model [5] and this needs particular attention. In the conventionally used  
19 3D solid FE formulation developed by Genta [5], the rotational moment of  
20 inertia is neglected. Such elements become inappropriate especially for thick

21 and/or large rotor in which these moments have a first-order influence on the  
22 structural dynamics [6, 7]. None of the above researches [1, 2, 3, 4] takes the  
23 inertial effects into consideration.

24 Models that account for rotational inertia effects have been developed in  
25 simpler structures such as a rotating beam [8] or a rotating Mindlin plate [9]  
26 equipped with rotational degrees of freedom. However, to the best of au-  
27 thors' knowledge, the investigation of rotational inertia effects on rotating  
28 structures using 3D solid FE formulation is very limited. The first attempt  
29 was presented by G eradin and Kill [6]. They introduced a particular particle-  
30 attached reference frame whose orientation was used to characterize the  
31 particle rotational motion. The rotation was defined by spatial derivatives  
32 of translational degrees of freedom. However, the axisymmetric hypothesis  
33 made prevents the application of its kinematic description to a more general  
34 case.

35 Commercial software, such as ANSYS [10] and NASTRAN [11], account  
36 for the inertial effects in their solid FE formulation only when the dynamics  
37 analysis is performed in a fixed (inertial) reference frame. However, most of  
38 the rotor dynamics models involving isotropic bearing system are developed  
39 in the rotating reference frame because it is convenient to express the equa-  
40 tions of motion using constant dynamic matrices (given in [12] for instance).  
41 The absence of rotational inertia for solid elements makes the derivation of  
42 these dynamic matrices a challenging task. This complexity has limited the  
43 use of these 2D and 3D elements for modeling rotor components [7].

44 The above review reveals the potential benefit of a 3D solid FE taking  
45 the rotational inertia effects into consideration in a general way as there is  
46 an industrial demand in both rotor design companies and commercial soft-  
47 ware developers. The aim of this paper is therefore to develop a new solid  
48 element involving these inertial effects. Its main contribution is to propose  
49 an enhanced 3D solid FE formulation that can lead to a more general and  
50 appropriate kinematic description of rotating structures.

51 The rotating reference frame approach introduced by G eradin [6] serves  
52 as the basis for the proposed development and is here extended to include  
53 nonlinear deformation generated by centrifugal force and rotational inertia  
54 effects. In order to avoid the axisymmetry hypothesis, a general approxima-  
55 tion of rotation-translation relation is introduced. In Section 2, the equations  
56 of motion, including the effects of the moment of inertia in rotating struc-  
57 tures, are established using Hamilton’s principle. A Total-Lagrangian for-  
58 mulation is applied to correctly predict the centrifugal-stiffening effect which  
59 is fundamental for accurate simulations under large spin-speed. The general  
60 formulation of the centrifugal stiffening developed in this section is also an  
61 original aspect of this paper. Finally, following the more classical procedure  
62 of FE discretization detailed in Section 3, the free vibration of different rotat-  
63 ing structures are analyzed in Section 4 to validate the proposed formulation.  
64 Results on the natural frequencies are compared with those obtained from  
65 analytical or semi-analytical solutions found in the literature.

## 66 2. Enhanced kinematics relation including rotational inertia effects

67 Gérardin and Kill in [6] first developed a new approach to formulate a fi-  
68 nite element of rotating structures. They defined a dynamic reference frame  
69 for each point in the body according to the fact that, in a flexible continuum,  
70 the deformation and angular velocity change from point to point. With an in-  
71 finitesimal displacement hypothesis, the Lagrangian and Eulerian description  
72 were considered as coincident. The objective of this section and novelty of  
73 this paper is to extent their approach into a more general and more versatile  
74 3D solid form with the least possible approximations.

### 75 2.1. Kinematics description

76 In this paper, we consider a general solid rotating with an imposed con-  
77 stant spin speed  $\Omega$  about an axis ( $Oz$ ) and want to express the system  
78 dynamics in the rotating reference frame. **The two frames** ( $O; \mathbf{x}, \mathbf{y}, \mathbf{z}$ ) and  
79 ( $O; \mathbf{x}_r, \mathbf{y}_r, \mathbf{z}_r$ ) in Fig. 1 denote respectively the stationary and rotating ref-  
80 erence frames. The position vector of a general point  $P$  in the stationary  
81 reference frame is related to its expression in the rotating reference frame  
82 with the orthogonal rotation matrix  $\mathbf{H}$  given as:

$$\mathbf{H} = \begin{bmatrix} \cos(\Omega t) & -\sin(\Omega t) & 0 \\ \sin(\Omega t) & \cos(\Omega t) & 0 \\ 0 & 0 & 1 \end{bmatrix} \quad (1)$$

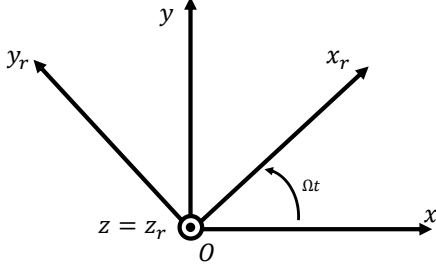


Figure 1: Stationary and rotating reference frames

83 Let consider an arbitrary material point  $P$  whose initial coordinate vector  
 84  $\mathbf{p}_i$ , with respect to the rotating reference, is written as:

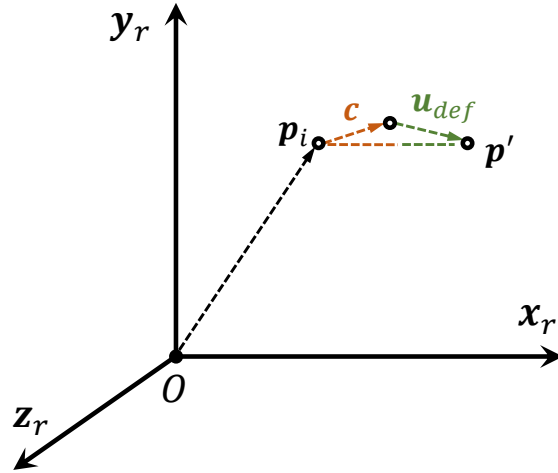
$$\mathbf{p}_i = \begin{bmatrix} x_0 & y_0 & z_0 \end{bmatrix}^T \quad (2)$$

85 The rigid body translation field  $\mathbf{c} = \begin{bmatrix} c_x & c_y & c_z \end{bmatrix}^T$  and the deformational  
 86 displacement field  $\mathbf{u}_{def} = \begin{bmatrix} u_{def} & v_{def} & w_{def} \end{bmatrix}^T$  are then introduced to move  
 87 particle from  $\mathbf{p}_i$  to  $\mathbf{p}'$  such that:

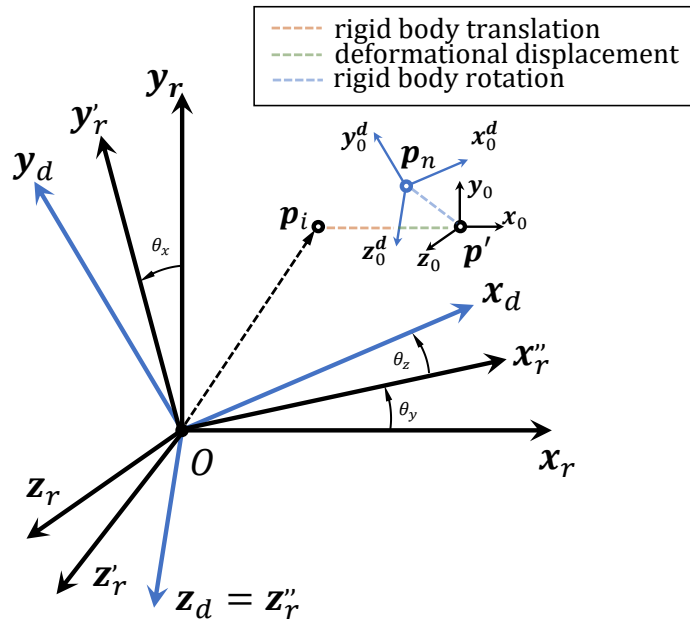
$$\mathbf{p}' = \mathbf{p}_i + \mathbf{u}_{def} + \mathbf{c} \quad (3)$$

88 This is illustrated in Fig. 2a. Subsequently, in order to associate each material  
 89 point with a particular rotational orientation, we define an auxiliary local  
 90 dynamic frame noted  $(\mathbf{p}_n; \mathbf{x}_0^d, \mathbf{y}_0^d, \mathbf{z}_0^d)$  attached to every material point  $\mathbf{p}_n$  in  
 91 the current configuration  $C_n$ . The transformation used to create the dynamic  
 92 reference frame follows the definition of 3D Euler rotations. These rotations,

93 whom details are illustrated in [Appendix B](#), are: a rotation  $\theta_x$  about the  
94  $\mathbf{x}_r$ -axis, a rotation  $\theta_y$  about the new  $\mathbf{y}_r$ -axis, and finally a  $\theta_x$  rotation  
95 about the new  $\mathbf{z}_d$ -axis. The above three successive rotations are similar to  
96 a rigid body rotation applied on each material particle (the corresponding  
97 transformation matrix  $\mathbf{R}$  is given in Eq. (B.1) in [Appendix B](#)).



(a) Initial deformations



(b) Summarized kinematics

Figure 2: Proposed kinematic relation

98 Due to the combined rigid body translation  $\mathbf{c}$ , rigid body rotations  $\mathbf{R}$   
 99 and deformational displacement  $\mathbf{u}_{def}$ , the general material point  $\mathbf{p}$  initially  
 100 located at  $\mathbf{p}_i$  is subsequently displaced to  $\mathbf{p}'$  and then transformed into the  
 101 current configuration  $\mathbf{p}_n$ . The coordinate vector of the particle in  $C_n$  with  
 102 respect to the rotating reference frame becomes (see Fig. 2b):

$$\mathbf{p}_n = \mathbf{R}\mathbf{p}' = \mathbf{R}(\mathbf{p}_i + \mathbf{u}_{def} + \mathbf{c}) \quad (4)$$

### 103 2.2. Kinetic energy analysis

104 The velocity  $\mathbf{v}_s$  of the general particle  $\mathbf{p}_n$  in  $C_n$  with respect to the sta-  
 105 tionary reference frame is given, using (4), by:

$$\mathbf{v}_s = \frac{d}{dt}(\mathbf{H}\mathbf{p}_n) = \dot{\mathbf{H}}\mathbf{R}\mathbf{p}' + \mathbf{H}\dot{\mathbf{R}}\mathbf{p}' + \mathbf{H}\mathbf{R}\dot{\mathbf{p}}' \quad (5)$$

106 where subscript  $\{ \}_s$  represents the stationary reference frame. The kinetic  
 107 energy of the structure, noted  $\Pi_0$ , is defined with:

$$\Pi_0 = \frac{1}{2} \int_{^0V} \mathbf{v}_s^T \mathbf{v}_s d^0V \quad (6)$$

108 where  $^0V$  represents the undeformed configuration. Using Eqs. (5) and (6)  
 109 gives the following expression for the kinetic energy:

$$\begin{aligned} \Pi_0 = \frac{1}{2} \int_{^0V} \left\{ \dot{\mathbf{p}}'^T \dot{\mathbf{p}}' + \mathbf{p}'^T \dot{\mathbf{R}}^T \dot{\mathbf{R}}\mathbf{p}' + \mathbf{p}'^T \mathbf{R}^T \dot{\mathbf{H}}^T \dot{\mathbf{H}}\mathbf{R}\mathbf{p}' \right. \\ \left. + 2\mathbf{p}'^T \mathbf{R}^T \dot{\mathbf{H}}^T \mathbf{H}\dot{\mathbf{R}}\mathbf{p}' + 2\mathbf{p}'^T \mathbf{R}^T \dot{\mathbf{H}}^T \mathbf{H}\mathbf{R}\dot{\mathbf{p}}' + 2\mathbf{p}'^T \dot{\mathbf{R}}^T \mathbf{R}\dot{\mathbf{p}}' \right\} d^0V \end{aligned} \quad (7)$$

110 In order to express the kinetic energy in a quadratic form in terms of  
 111 the proposed generalized coordinates  $\mathbf{q}_0$  ( $\mathbf{q}_0 = \left[ \mathbf{u}_{def}^T, \theta_x, \theta_y, \theta_z, \mathbf{c}^T \right]^T$ ) and  
 112 their time-derivatives  $\dot{\mathbf{q}}_0$ , the transformation  $\mathbf{R}$  shall be limited to a second-  
 113 order approximation in terms of the elemental rotations  $(\theta_x, \theta_y, \theta_z)$ . This  
 114 approximation is explained in [Appendix B](#). Substituting the expansion of  
 115  $\mathbf{R}$  given in Eq. (B.4) into Eq. (7) and neglecting the high-order terms with  
 116 respect to  $\mathbf{q}_0$  and  $\dot{\mathbf{q}}_0$  gives the following kinetic energy which is in  $\mathbf{q}_0$ -related  
 117 quadratic form:

$$\begin{aligned}
 \Pi_0^{quad} = \int_{0V} \left\{ \frac{1}{2} \dot{\mathbf{q}}_0^T \mathbf{M}_0 \dot{\mathbf{q}}_0 + \Omega \dot{\mathbf{q}}_0^T \mathbf{G}_0 \mathbf{q}_0 + \frac{1}{2} \Omega^2 \mathbf{q}_0^T \mathbf{K}_{0,\Omega} \mathbf{q}_0 \right. \\
 \left. + \Omega \mathbf{f}_1^T \dot{\mathbf{q}}_0 + \Omega^2 \mathbf{f}_2^T \mathbf{q}_0 + E \right\} d^0V
 \end{aligned} \tag{8}$$

118 where  $\mathbf{M}_0$ ,  $\mathbf{G}_0$  and  $\mathbf{K}_{0,\Omega}$  are respectively the mass, gyroscopic and spin-  
 119 softening stiffness matrices with respect to  $\mathbf{q}_0$ . The term in  $\mathbf{f}_1$  will vanish in  
 120 the Lagrange's equation because  $\mathbf{f}_1$  is time-independent. Once differentiated  
 121 with respect to  $\mathbf{q}_0$ , the term in  $\mathbf{f}_2$  will generate the centrifugal force. The  
 122 last term  $E$  is a constant and represents the rigid-body kinetic energy due to  
 123 the imposed uniform rotation  $\Omega$  about the  $\mathbf{z}$ -axis. The explicit expressions  
 124 of matrices, vectors and constant terms in Eq.(8) are given in [Appendix C](#).  
 125 All three types of motions (deformation, rigid-body translational and rigid-  
 126 body rotational) contribute to these matrices. The effects of Coriolis and  
 127 spin-softening associated with the rotational motion of spin speed  $\Omega$  are well  
 128 taken into account in  $\Pi_0^{quad}$ . The proposed kinematics therefore offers a

129 general description able to model rotating structures.

130 The formulation proposed in this paper is built using only the trans-  
 131 lational degrees of freedom of solid finite elements. Therefore, it will be  
 132 necessary to establish a relationship between the components of  $\mathbf{q}_0$  and these  
 133 degrees of freedom. This is the focus of the next section.

### 134 2.3. Continuum kinematic approximation

135 An efficient approximation of  $\mathbf{q}_0$  can be derived from the basic definition  
 136 of deformation in continuum mechanics. The position  $\mathbf{p}_n$  of the particle in the  
 137 current configuration can also be defined with a simple general translation  
 138 field  $\mathbf{u}$  which coincides with the description of the degrees of freedom of the  
 139 solid finite element such that:

$$\mathbf{p}_n = \mathbf{p}_i + \mathbf{u} \quad (9)$$

where  $\mathbf{u} = \begin{bmatrix} u_r & v_r & w_r \end{bmatrix}^T$  represents the general translations of the particle with respect to the rotating reference frame. By introducing the definition of general in-homogeneous deformation [13] in classical continuum kinematics, we may write:

$$\mathbf{p}_n = \mathbf{F}\mathbf{p}_i + \mathbf{r} \quad (10a)$$

$$= \mathbf{R}\mathbf{U}\mathbf{p}_i + \mathbf{r} \quad (10b)$$

$$= \mathbf{R}(\mathbf{p}_i + \underbrace{(\mathbf{U} - \mathbf{I})\mathbf{p}_i}_{\mathbf{u}_{def}} + \underbrace{\mathbf{R}^T\mathbf{r}}_{\mathbf{c}}) \quad (10c)$$

140 where:

$$\mathbf{F} = [\nabla \mathbf{p}_n] = \mathbf{I} + [\nabla \mathbf{u}] \quad (11)$$

141 In these expressions,  $\nabla$  is the gradient operator,  $\mathbf{F}$  represents the deformation  
 142 gradient (second-order tensor) [14],  $\mathbf{r}$  is the spatial non-uniform rigid body  
 143 translation [13].  $\mathbf{R}$  and  $\mathbf{U}$  are respectively the rigid body rotation tensor and  
 144 the right stretch tensor obtained from the polar decomposition of  $\mathbf{F} = \mathbf{R}\mathbf{U}$ .

145 Comparing Eq. (10c) with Eq. (4) shows that  $\mathbf{R}$  represents the same  
 146 rigid body rotation in both kinematics description. By equating Eq. (9) and  
 147 Eq. (10),  $\mathbf{u}_{def}$  and  $\mathbf{c}$  can be given in form of continuum mechanics terms as:

$$\begin{aligned} \mathbf{u}_{def} &= (\mathbf{U} - \mathbf{I}) \mathbf{p}_i = (\mathbf{R}^T \mathbf{F} - \mathbf{I}) \mathbf{p}_i \\ \mathbf{c} &= \mathbf{R}^T \mathbf{r} = \mathbf{R}^T (\mathbf{I} - \mathbf{F}) \mathbf{p}_i + \mathbf{R}^T \mathbf{u} \end{aligned} \quad (12)$$

148 Both expressions in Eq. (12) are of second-order in the general translation  
 149 field  $\mathbf{u}$ . In order to keep the kinetic energy expression in Eq. (8) in a quadratic  
 150 form, Eq. (12) should be approximated into a first-order form with respect  
 151 to  $\mathbf{u}$  before substituting the  $\mathbf{q}_0$ -value into Eq. (8). Following the infinitesimal  
 152 deformation theory [15], the following consistent linearization of Eq. (12) will  
 153 be used:

$$\begin{aligned} \tilde{\mathbf{u}}_{def} &= \left( [\nabla \mathbf{u}] + [\boldsymbol{\omega}]^T \right) \mathbf{p}_i \\ \tilde{\mathbf{c}} &= -[\nabla \mathbf{u}] \mathbf{p}_i + \mathbf{u} \end{aligned} \quad (13)$$

154 where  $[\nabla \mathbf{u}]$  is the displacement gradient matrix and  $[\boldsymbol{\omega}]$  is the skew-symmetric  
 155 rotation tensor. The detailed analytical developments can be found in [Ap-](#)

156 [pendix D](#).

157 We may note that the  $\mathbf{R}$ -matrix in Eq. (4), parameterized by the angles  
158  $\theta_x$ ,  $\theta_y$  and  $\theta_z$ , and the  $\mathbf{R}$ -matrix in Eq. (10) extracted from deformation  
159 gradient describe identical kinematics. Thus, it is possible to relate the angles  
160  $\theta_x$ ,  $\theta_y$  and  $\theta_z$  to the translations at the point of interest by:

$$\begin{aligned}\theta_x(\mathbf{p}_i) &= \frac{1}{2} \left( \frac{\partial w_r}{\partial y_0} - \frac{\partial v_r}{\partial z_0} \right) \\ \theta_y(\mathbf{p}_i) &= \frac{1}{2} \left( \frac{\partial u_r}{\partial z_0} - \frac{\partial w_r}{\partial x_0} \right) \\ \theta_z(\mathbf{p}_i) &= \frac{1}{2} \left( \frac{\partial v_r}{\partial x_0} - \frac{\partial u_r}{\partial y_0} \right)\end{aligned}\tag{14}$$

161 Similar rotation-translation relations can also be found in various refer-  
162 ences [5, 16]. However, only a few of them provide full coupled expressions  
163 and a detailed demonstration. In order to verify the proposed kinematic re-  
164 lation of Eq. (14), a different explicit development can be found in [Appendix](#)  
165 [E](#). One may also notice that the approximated rotations in Eq. (14) are first-  
166 order of general translation. Thus, for the sake of simplicity, we can keep  
167 the rotation-related quadratic kinetic energy terms of Eq. (8) as a function  
168 of  $(\theta_x, \theta_y, \theta_z)$  until the discretization step. It is only at this point that the  
169 spatial derivatives of Eq. (14) will be used.

170 The kinetic energy in Eq. (8) is then expressed as a quadratic form in the  
171 general translation  $\mathbf{u}$  by substituting  $\tilde{\mathbf{u}}_{def}$  and  $\tilde{\mathbf{c}}$  from Eq. (13) into Eq. (8).  
172 It gives:

$$\Pi^{quad} = \Pi_0^v + \Pi_1^v + \Pi_2^v + \Pi_3^v\tag{15}$$

173 The different components of  $\Pi^{quad}$  are detailed next:

- 174 • the relative kinetic energy:

$$\Pi_0^v = \frac{1}{2} \int_{0V} \rho (\dot{u}_r^2 + \dot{v}_r^2 + \dot{w}_r^2) d^0V \quad (16)$$

175 It will provide the mass matrix after discretization.

- the coupling kinetic energy, function of  $\Omega$ :

$$\begin{aligned} \Pi_1^v = \Omega \left[ \int_{0V} \rho(\mathbf{p}_i) \left( \dot{v}_r(x_0 + u_r) - \dot{u}_r(y_0 + v_r) + x_0(\dot{u}_r\theta_z + \dot{\theta}_z u_r) \right. \right. \\ \left. \left. - y_0(\dot{w}_r\theta_y + \dot{\theta}_y w_r) + y_0^2/2(\dot{\theta}_x\theta_y + \dot{\theta}_y\theta_x) - x_0^2/2(\dot{\theta}_x\theta_y + \dot{\theta}_y\theta_x) \right. \right. \\ \left. \left. + x_0 y_0(\dot{\theta}_x\theta_x - \dot{\theta}_y\theta_y) - \frac{x_0 z_0}{2}(\dot{\theta}_y\theta_z + \dot{\theta}_y\theta_z) + \frac{y_0 z_0}{2}(\dot{\theta}_x\theta_z + \dot{\theta}_x\theta_z) \right) d^0V \right] \end{aligned} \quad (17)$$

176 It will generate the gyroscopic matrix after discretization.

- the spin softening kinetic energy, function of  $\Omega^2$ :

$$\begin{aligned} \Pi_2^v = \frac{1}{2} \Omega^2 \left[ \int_{0V} \rho(\mathbf{p}_i) \left( (x_0^2 + u_r^2) + (y_0^2 + v_r^2) \right. \right. \\ \left. \left. + 2w_r(x_0\theta_y - y_0\theta_x) + 2\theta_z(y_0 u_r - x_0 v_r) \right. \right. \\ \left. \left. + (\theta_x y_0 - \theta_y x_0)^2 + \theta_z^2(x_0^2 + y_0^2) \right. \right. \\ \left. \left. - x_0 z_0 \theta_x \theta_z - y_0 z_0 \theta_y \theta_z \right) d^0V \right] \end{aligned} \quad (18)$$

177 After discretization, this will provide not only the standard spin-softening  
 178 matrix but also original terms that couple position and rotation.

179 • the centrifugal kinetic energy:

$$\Pi_3^v = \Omega^2 \int_{0V} \rho(\mathbf{p}_i) \left[ x_0 u_r + y_0 v_r + \frac{1}{2} (x_0^2 + y_0^2) \right] d^0V \quad (19)$$

180 According to Lagrange's equation, this term will give rise to an inertial  
 181 force  $\mathbf{f}_\Omega$  given by:

$$\mathbf{f}_\Omega = \Omega^2 \int_{0V} [\rho(\mathbf{p}_i) \mathbf{A}\mathbf{p}_i] d^0V \quad (20)$$

182 where  $\mathbf{A} = \text{diag}([1, 1, 0])$ <sup>1</sup>.  $\mathbf{f}_\Omega$  is a geometry-dependent centrifugal  
 183 force vector. It can be treated like a static load. The force  $\mathbf{f}_\Omega$  depends  
 184 simultaneously on the updated mass density  $\rho(\mathbf{p}_i)$  and on the updated  
 185 mass particle distribution  $\mathbf{p}_i$ . The particular effect of this term will be  
 186 detailed in Section 2.5.

187 Rotational effects, due to the consideration of the rotational motion in the  
 188 kinematics description, are now present in both coupling kinetic energy and  
 189 centrifugal softening kinetic energy. This is not the case in a purely linear  
 190 description of the kinematics. In Section 2.4, the extended rotation-included  
 191 kinematic relation will be applied into strain energy evaluation.

---

<sup>1</sup>diag is the diagonal matrix operator

192 *2.4. Strain energy analysis*

193 We consider in this paper the dynamic behavior of rotating systems at  
 194 high spin speed with respect to a rotating reference frame. It is crucial to  
 195 calculate the pre-stressed state of the system, deformed under centrifugal  
 196 force, around which the final equation of motion of the rotating structure is  
 197 established. In the case that the spin speed is important and the associated  
 198 centrifugal deformation is large, the conventional linear perturbation method  
 199 based on in-extensible model is no longer accurate. Thus, in order to pre-  
 200 cisely predict the static displacement generated by the centrifugal force and  
 201 to accurately evaluate the centrifugal stiffening effect, the Total-Lagrangian  
 202 formulation is adopted in this paper.

203 The kinematic relation  $\tilde{\mathbf{p}}_{n,d}$  of Eq. (E.2) is projected into the rotating ref-  
 204 erence frame with the transformation matrix in Eq. (B.4) in order to evaluate  
 205 the strain energy. Removing higher order terms yields to the second-order  
 206 approximation:

$$\tilde{\mathbf{p}}_{n,r} = \begin{bmatrix} x_0 \\ y_0 \\ z_0 \end{bmatrix} + \begin{bmatrix} u_r \\ v_r \\ w_r \end{bmatrix} + \begin{bmatrix} 0 & -\theta_z & \theta_y \\ \theta_z & 0 & -\theta_x \\ -\theta_y & \theta_x & 0 \end{bmatrix} \begin{bmatrix} u_r \\ v_r \\ w_r \end{bmatrix} - \frac{1}{2} \begin{bmatrix} 0 & -\theta_z & \theta_y \\ \theta_z & 0 & -\theta_x \\ -\theta_y & \theta_x & 0 \end{bmatrix}^2 \begin{bmatrix} x_0 \\ y_0 \\ z_0 \end{bmatrix} \quad (21)$$

207 where  $\tilde{\mathbf{p}}_{n,r}$  represents the coordinate vector of a particle in the current con-  
 208 figuration  $C_n$ , expressed in the rotating reference frame. The conventional  
 209 solid element formulation for rotor dynamics analysis in [5, 17, 18] includes

210 the first and second terms of Eq. (21). By introducing the local dynamic  
 211 frame, the second-order rotation-related (third and fourth terms) terms are  
 212 also taken into account leading to a more accurate relation to perform the  
 213 strain energy analysis.

214 Using this extended kinematic relation, some forces and displacements are  
 215 applied on the solid so that its geometry changes from the initial configuration  
 216 ( $C_0$ ) to the current configuration ( $C_n$ ). The one-to-one mapping from a  
 217 particular material point in ( $C_0$ ) with coordinate vector  $\mathbf{p}_i$  to a point with  
 218 coordinate vector  $\tilde{\mathbf{p}}_{n,r}$ , given in Eq. (21), in the deformed geometry can also  
 219 be written as:

$$\tilde{\mathbf{p}}_{n,r} = \mathbf{p}_i + \tilde{\mathbf{u}}(\mathbf{p}_i, t) \quad (22)$$

220 where the displacement vector  $\tilde{\mathbf{u}}$  of a particle  $P$ , expressed in the rotating  
 221 reference frame, is simply the difference between the final position  $\tilde{\mathbf{p}}_{n,r}$  and  
 222 the initial position  $\mathbf{p}_i$ . Therefore,  $\tilde{\mathbf{u}}$  can be expressed as:

$$\tilde{\mathbf{u}} = \begin{bmatrix} u_r \\ v_r \\ w_r \end{bmatrix} + \begin{bmatrix} 0 & -\theta_z & \theta_y \\ \theta_z & 0 & -\theta_x \\ -\theta_y & \theta_x & 0 \end{bmatrix} \begin{bmatrix} u_r \\ v_r \\ w_r \end{bmatrix} - \frac{1}{2} \begin{bmatrix} 0 & -\theta_z & \theta_y \\ \theta_z & 0 & -\theta_x \\ -\theta_y & \theta_x & 0 \end{bmatrix}^2 \begin{bmatrix} x_0 \\ y_0 \\ z_0 \end{bmatrix} \quad (23)$$

223 According to the Total-Lagrangian formulation, the strain measure of the  
 224 flexible body in the rotating reference frame is defined by Green-Lagrangian  
 225 (G-L) strains with respect to the initial configuration. Using the G-L strain  
 226 measure referencing to  $C_0$ , the total strain energy  $\Pi_s$  of the deformed body

227 is [19]:

$$\Pi_s = \int_{^0V} \left[ \frac{1}{2} \mathbf{e}(\mathbf{p}_i, \tilde{\mathbf{u}})^T \mathbf{C} \mathbf{e}(\mathbf{p}_i, \tilde{\mathbf{u}}) \right] d^0V \quad (24)$$

228 where  $^0V$  represents the volume domain of the initial undeformed configura-  
 229 tion  $C_0$ ;  $\mathbf{e}$  is the G-L strain tensor written in a vector form; and  $\mathbf{C}$  is the  
 230 constitutive matrix of the material assumed to be linear elastic, homogeneous  
 231 and isotropic, defined using Lamé's coefficients  $\lambda$  and  $\mu$  as:

$$\mathbf{C} = \begin{bmatrix} \lambda + 2\mu & \lambda & \lambda & 0 & 0 & 0 \\ & \lambda + 2\mu & \lambda & 0 & 0 & 0 \\ & & \lambda + 2\mu & 0 & 0 & 0 \\ & & & \mu & 0 & 0 \\ & \text{symm.} & & & \mu & 0 \\ & & & & & \mu \end{bmatrix}. \quad (25)$$

232 According to the Lagrange's equation, the internal elastic force  $\mathbf{f}_s$  can be  
 233 obtained by differentiating the total strain energy (Eq. (24)) with respect to  
 234 the displacement vector in the rotating reference frame  $\mathbf{u}_r$ . This gives:

$$\mathbf{f}_s(\mathbf{u}_r) = \frac{\partial}{\partial \mathbf{u}_r} \left( \int_{^0V} \left[ \frac{1}{2} \mathbf{e}(\mathbf{p}_i, \tilde{\mathbf{u}})^T \mathbf{C} \mathbf{e}(\mathbf{p}_i, \tilde{\mathbf{u}}) \right] d^0V \right) \quad (26)$$

235 In order to equilibrate the static load generating from the centrifugal  
 236 force, the iterative Newton-Raphson method will be used. It then needs the

237 tangent elastic force matrix  $\mathbf{K}_s$  given by:

$$\mathbf{K}_s = \frac{\partial \mathbf{f}_s}{\partial \mathbf{u}_r} \quad (27)$$

238 Eq. (26) gives the internal elastic force. However, in order to evaluate the  
239 centrifugal stiffening effect, one must still carefully define the pre-stress due  
240 to centrifugal force. This will be detailed in the next section.

#### 241 *2.5. Centrifugal stiffening effect evaluation*

242 The above total strain energy and its corresponding elastic force are ex-  
243 pressed referencing to the initial configuration  $C_0$ . However, because the  
244 inertial force (centrifugal load) of the material point is function of both its  
245 current position coordinates and its current mass density (which changes  
246 with deformation) [20], the centrifugal load should also be expressed with  
247 respect to the current configuration  $C_n$ . Thus, in order to accurately solve  
248 the centrifugal load corresponding static equation, a Total-Lagrangian (T-  
249 L) based process is proposed where the initial position becomes the current  
250 configuration state prior to some incremental change. T-L approach offers  
251 advantages since the initial configuration remains constant which simplifies  
252 formulation and computation. Following the same kinematic relation, the  
253 expression of the centrifugal force density of the displaced point  $P$ , noted  
254  $\mathbf{f}_\Omega^p$ , as a function of the displacement is given by

$$\mathbf{f}_\Omega^p(\mathbf{p}_i + \tilde{\mathbf{u}}) = \Omega^2 \rho(\mathbf{p}_i + \tilde{\mathbf{u}}) \mathbf{A}(\mathbf{p}_i + \tilde{\mathbf{u}}) \quad (28)$$

255 where  $\rho$  is the mass density of this particular point  $P$  in the current deformed  
 256 configuration. The centrifugal force applied on the deformed body is then  
 257 expressed as:

$$\mathbf{f}_\Omega = \int_{{}^nV} [\Omega^2 \rho(\mathbf{p}_i + \tilde{\mathbf{u}}) \mathbf{A}(\mathbf{p}_i + \tilde{\mathbf{u}})] d^nV \quad (29)$$

258 where  ${}^nV$  represents the volume of the current deformed configuration  $C_n$ .  
 259 Using the following mass conservation property [21]:

$$\int_{{}^0V} [\rho(\mathbf{p}_i + \tilde{\mathbf{u}}) J - \rho_0] d^0V = 0 \quad \text{or} \quad \rho(\mathbf{p}_i + \tilde{\mathbf{u}}) J - \rho_0 = 0 \quad (30)$$

260 where  $J$  is the determinant of the deformation gradient (equivalent to the  
 261 change of volume), and changing the integration domain ( $d^nV = Jd^0V$ ), the  
 262 expression of the centrifugal force (29) can be finally transformed into a form  
 263 of integration over  $C_0$  with a constant mass density  $\rho_0$ :

$$\mathbf{f}_\Omega = \int_{{}^0V} \left[ \Omega^2 \frac{\rho_0}{J} \mathbf{A}(\mathbf{p}_i + \tilde{\mathbf{u}}) \right] J d^0V = \int_{{}^0V} [\Omega^2 \rho_0 \mathbf{A}(\mathbf{p}_i + \tilde{\mathbf{u}})] d^0V \quad (31)$$

264 This later expression gives a direct relationship between the centrifugal  
 265 load and the displacement taking account for both the current material point  
 266 coordinates and its actualized mass density. The internal elastic force coming  
 267 from the elastic deformation is equal to the centrifugal force supplemented  
 268 by all other external forces. This gives the following equilibrium at a given  
 269 spin speed:

$$\mathbf{f}_s(\mathbf{u}_r) = \mathbf{f}_\Omega(\mathbf{u}_r, \Omega) + \mathbf{f}_{ext} \quad (32)$$

270 where  $\mathbf{f}_{ext}$  is the applied external forces and  $\mathbf{u}_r$  is the unknown initial dis-  
 271 placement vector that equilibrates both forces. To solve the above static  
 272 boundary value problem, the iterative Newton-Raphson method [22] can be  
 273 applied.

274 After finding the converged displacement  $\mathbf{u}_r$ , the centrifugal-stiffening  
 275 effect can be correctly evaluated. The updated mass density will be reused  
 276 in the following dynamic analysis in order to improve the model accuracy. In  
 277 other words, the final set of dynamic matrices used to perform the vibration  
 278 analysis are established around the centrifugal-equilibrium configuration  $C_{eq}$ .  
 279 This configuration may have a large change of mass distribution when a high  
 280 spin speed is applied. Substituting the found initial displacement  $\mathbf{u}_r$  into  
 281 Eq. (30) gives us the expression of the updated mass distribution as:

$$\rho = \frac{\rho_0}{J(\mathbf{u}_r, \mathbf{p}_i)} \quad (33)$$

282 The kinematics presented in Section 2.1 will then be applied on the new  
 283 ‘initial’ configuration  $C_{eq}$  with a new updated mass distribution calculated  
 284 with Eq. (33).

285 In the numerical applications presented in Section 4, the changes of mass  
 286 density due to the centrifugal pre-stress are all naturally embedded in the  
 287 numerical process.

### 288 3. Finite element discretization

289 There are many different approaches to discretize a solid in a FE method [23,  
290 24]. In this paper, the 20-node second order **hexahedron** element with uni-  
291 form reduced numerical integration technique is applied. This element has 8  
292 nodes on corners and 12 mid-side nodes, with only translational degrees of  
293 freedom. Its advantages are its accuracy in 3D complex geometry modeling,  
294 its robustness in shear and volume locking and its tolerance under coarse  
295 mesh. By opposition to first order elements (4-node tetrahedral element or  
296 8-node hexahedron element), the 20-node second order element does not re-  
297 quire an enhanced strain technique [25]. This simplifies its strain-related  
298 formulation.

#### 299 3.1. Iso-parametrized mapping

300 Two different discretized models are used for respectively the centrifugal  
301 stiffening analysis and the dynamic analysis. The centrifugal stiffening  
302 model, based on T-L formulation, is discretized upon  $C_0$ . On the contrary,  
303 the discretized model for the dynamic analysis is based on the new centrifugal  
304 equilibrium configuration  $C_{eq}$ . Particular attention must be paid to update  
305 the change of mass density in the discretized dynamic model.

##### 306 3.1.1. Discretized centrifugal stiffening model

307 In the centrifugal stiffening analysis, the initial configuration  $C_0$  is used  
308 as basic reference. The material point coordinates vector  $\mathbf{p}_i$  in  $C_0$  and its

309 corresponding translational displacement vector  $\mathbf{u}$  are interpolated using a  
 310 20-node iso-parametric formulation. They are expressed by:

$$\mathbf{p}_i = \sum_{i=1}^{20} \varphi_i(\xi, \eta, \zeta) \mathbf{x}_i^0 \quad \text{and} \quad \mathbf{u} = \sum_{i=1}^{20} \varphi_i(\xi, \eta, \zeta) \mathbf{u}_i \quad (34)$$

311 where  $\varphi_i$  is the  $i$ -th nodal shape function (explicitly expressed in [10] for  
 312 instance) with local coordinates  $-1 \leq \xi, \eta, \zeta \leq 1$ .  $\mathbf{x}_i^0$  represents the  $i$ -th nodal  
 313 coordinates in  $C_0$  and  $\mathbf{u}_i$  denotes the  $i$ -th nodal translational displacement  
 314 vector with respect to its initial coordinates  $\mathbf{x}_i^0$  in  $C_0$ .

315 In order to realize the reduced integration operation, one defines the Jaco-  
 316 bian mapping matrix  $\mathbf{J}_0$  from the initial configuration  $C_0$  to the isoparametric  
 317 parenting reference by taking the derivative of  $\mathbf{p}_i$  as [22]:

$$\mathbf{J}_0(\mathbf{p}_i, \boldsymbol{\xi}) = \frac{\partial \mathbf{p}_i}{\partial \boldsymbol{\xi}} = \sum_{i=1}^{20} \mathbf{x}_i^0 \frac{\partial \varphi_i}{\partial \boldsymbol{\xi}} \quad (35)$$

318 where  $\boldsymbol{\xi}$  contains the three local coordinates. With the use of the above  
 319 defined Jacobian  $\mathbf{J}_0$ , the integration over the element domain in the initial  
 320 configuration  ${}^0V^e$  can be converted into the integration over the isoparametric  
 321 reference element. This is achieved using the following relation:

$$\int_{{}^0V^e} d^0V^e = \iiint_{-1}^{+1} \det(\mathbf{J}_0) d\xi d\eta d\zeta \quad (36)$$

322 One can also express the discretized form of the displacement gradient

323  $\partial \mathbf{u} / \partial \mathbf{p}_i$  as:

$$\frac{\partial \mathbf{u}}{\partial \mathbf{p}_i} = \sum_{i=1}^{20} \mathbf{u}_i \frac{\partial \varphi_i}{\partial \boldsymbol{\xi}} \mathbf{J}_0^{-1} \quad (37)$$

324 *3.1.2. Discretized dynamic model*

325 Following the explanation given in Section 2, it is possible to get the  
 326 equilibrium configuration  $C_{eq}$  by updating the mass distribution (Eq. (33))  
 327 and equilibrating the centrifugal force. In this section, we consider that the  
 328 effect of change of geometry has already been taken into account and will  
 329 define the dynamics governing equation on  $C_{eq}$ .

330 Assuming that  $\mathbf{u}$  is known after resolving the boundary value problem  
 331 (Eq. (32)), the material point  $P$ 's coordinates vector  $\mathbf{x}$  and its related trans-  
 332 lational displacement vector  $\mathbf{u}_r$  can be interpolated with nodal coordinates  
 333 as:

$$\mathbf{x} = \sum_{i=1}^{20} \varphi_i(\xi, \eta, \zeta) \mathbf{x}_i^{eq} \quad \text{and} \quad \mathbf{u}_r = \sum_{i=1}^{20} \varphi_i(\xi, \eta, \zeta) \mathbf{u}_i^r \quad (38)$$

334 where  $\mathbf{x}_i^{eq}$  is the element's  $i$ -th node's position vector in  $C_{eq}$ . Using the  
 335 same technique as the one explained in Section 3.1.1, the mapping from the  
 336 physical configuration  $C_{eq}$  to the isoparametric reference, and the discretized  
 337 form of the displacement gradient with respect to  $C_{eq}$  are given by:

$$\mathbf{J}_0^{eq}(\mathbf{x}, \boldsymbol{\xi}) = \frac{\partial \mathbf{x}}{\partial \boldsymbol{\xi}} = \sum_{i=1}^{20} \mathbf{x}_i^{eq} \frac{\partial \varphi_i}{\partial \boldsymbol{\xi}} \quad \text{and} \quad \frac{\partial \mathbf{u}_r}{\partial \mathbf{x}} = \sum_{i=1}^{20} \mathbf{u}_i^r \frac{\partial \varphi_i}{\partial \boldsymbol{\xi}} (\mathbf{J}_0^{eq})^{-1} \quad (39)$$

338 *3.2. General equation of motion and derivation of its matrices*

339 After substituting Eqs. (38) and (39) into the quadratic form of the kinetic  
 340 energy (Eqs. (16), (17) and (18)) and applying Lagrange's equations, the  
 341 motion of the solid linearized around the centrifugal stiffened equilibrium  
 342 configuration can be defined with the following differential equation:

$$\mathbf{M}\{\ddot{u}_i^r\}_r + \mathbf{G}\{\dot{u}_i^r\}_r + (\mathbf{K}_s(\{x_i^{eq}\}) + \mathbf{K}_\Omega)\{u_i^r\} = \mathbf{0} \quad (40)$$

343 The expression of  $\mathbf{K}_s$  was directly given in Eq. (27).

344 For the sake of simplicity, in the following detailed expression of the  
 345 matrices  $\mathbf{M}$ ,  $\mathbf{G}$  and  $\mathbf{K}_\Omega$ , we will employ the notations:  $\mathbf{N} = \{\varphi_i\}$  is the  
 346 vector of element's shape functions ;  $\mathbf{N}_x = \{\varphi_{i,x}\}$ ,  $\mathbf{N}_y = \{\varphi_{i,y}\}$  and  $\mathbf{N}_z =$   
 347  $\{\varphi_{i,z}\}$  are respectively the vector of spatial derivative of shape functions along  
 348  $x$ -direction,  $y$ -direction and  $z$ -direction. All the above spatial differentiations  
 349 are with respect to the centrifugal-stiffened equilibrium configuration  $C_{eq}$   
 350 which can be evaluated by using Eq. (39). Finally,  $(x, y, z)$  represents the  
 351 position of a general particle in the solid element. Using the above mentioned  
 352 notations, the characteristic matrices of Eq. (40) are:

- 353 • the mass matrix  $\mathbf{M}$ :

$$\mathbf{M} = \iiint_{-1}^{+1} \rho_0 / \det \mathbf{J}(\mathbf{x}, \mathbf{p}_i) \begin{bmatrix} \mathbf{N}^T \mathbf{N} & \mathbf{0} & \mathbf{0} \\ \mathbf{0} & \mathbf{N}^T \mathbf{N} & \mathbf{0} \\ \mathbf{0} & \mathbf{0} & \mathbf{N}^T \mathbf{N} \end{bmatrix} \det \mathbf{J}(\mathbf{x}, \boldsymbol{\xi}) \, d\xi \, d\eta \, d\zeta \quad (41)$$

354 where  $\det \mathbf{J}(\mathbf{x}, \mathbf{p}_i)$  is the change of volume calculated from Eq. (33).

355 • the gyroscopic matrix  $\mathbf{G}$ :

$$\mathbf{G} = \iiint_{-1}^{+1} \Omega \rho_0 / \det \mathbf{J}(\mathbf{x}, \mathbf{p}_i) \begin{bmatrix} \mathbf{0} & -2\mathbf{N}^T \mathbf{N} & \mathbf{0} \\ 2\mathbf{N}^T \mathbf{N} & \mathbf{0} & \mathbf{0} \\ \mathbf{0} & \mathbf{0} & \mathbf{0} \end{bmatrix} \det \mathbf{J}(\mathbf{x}, \boldsymbol{\xi}) \, d\xi \, d\eta \, d\zeta \quad (42)$$

356 • and the spin-softening stiffness matrix  $\mathbf{K}_\Omega$ :

$$\mathbf{K}_\Omega = \iiint_{-1}^{+1} \Omega^2 \rho_0 / \det \mathbf{J}(\mathbf{x}, \mathbf{p}_i) \mathbf{G}^T \mathbf{K}_\Omega^{\text{core}} \mathbf{G} \det \mathbf{J}(\mathbf{x}, \boldsymbol{\xi}) \, d\xi \, d\eta \, d\zeta \quad (43)$$

357 where the matrix of rotation-inclusion  $\mathbf{G}$  is:

$$\mathbf{G} = \begin{bmatrix} \mathbf{N} & \mathbf{0} & \mathbf{0} \\ \mathbf{0} & \mathbf{N} & \mathbf{0} \\ \mathbf{0} & \mathbf{0} & \mathbf{N} \\ \mathbf{0} & -\mathbf{N}_z/2 & \mathbf{N}_y/2 \\ \mathbf{N}_z/2 & \mathbf{0} & -\mathbf{N}_x/2 \\ -\mathbf{N}_y/2 & \mathbf{N}_x/2 & \mathbf{0} \end{bmatrix} \quad (44)$$

358

and the core spin-softening matrix  $\mathbf{K}_\Omega^{\text{core}}$  is:

$$\mathbf{K}_\Omega^{\text{core}} = \begin{bmatrix} 1 & 0 & 0 & 0 & 0 & y \\ 0 & 1 & 0 & 0 & 0 & -x \\ 0 & 0 & 0 & -y & x & 0 \\ 0 & 0 & -y & y^2 & -xy & -(xz)/2 \\ 0 & 0 & x & -xy & x^2 & -(yz)/2 \\ y & -x & 0 & -(xz)/2 & -(yz)/2 & x^2 + y^2 \end{bmatrix} \quad (45)$$

359

360

361

362

The major difference in the proposed formulation compared with conventional solid FE for rotating structures [1, 2, 5] lies in the spin-stiffness matrix  $\mathbf{K}_\Omega$  of Eq. (43). In these references, the spin-stiffness matrix used is defined with:

$$\mathbf{K}_\Omega = \int_{-1}^{+1} \int_{-1}^{+1} \int_{-1}^{+1} \Omega^2 \rho_0 \tilde{\mathbf{G}}^T \tilde{\mathbf{K}}_\Omega^{\text{core}} \tilde{\mathbf{G}} \det \mathbf{J}(\mathbf{x}, \boldsymbol{\xi}) \, d\xi \, d\eta \, d\zeta \quad (46)$$

363

where  $\tilde{\mathbf{G}}$  and  $\tilde{\mathbf{K}}_\Omega^{\text{core}}$  contains only the top three components of  $\mathbf{G}$  and  $\mathbf{K}_\Omega^{\text{core}}$ .

364

365

366

367

In practical applications, once the centrifugal stiffened stationary configuration is determined, the natural frequencies and mode shapes of the rotating model can be calculated by solving the general equation of motion (40) in state-space.

368

#### 4. Numerical application

369

370

In this section, the natural frequencies of different rotating structures are calculated with the proposed formulation and compared with analytical

371 expression or conventional FE method.

372 *4.1. Rotating rigid disk*

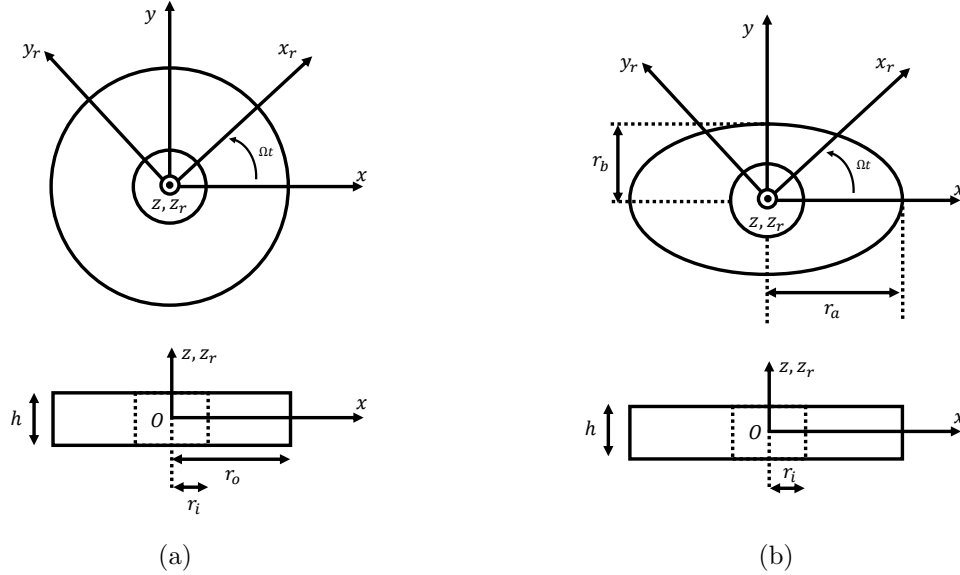


Figure 3: Rotating rigid disk configurations: (a) circular disk, (b) elliptic disk

373 The proposed enhanced solid element is first applied to a rotating cir-  
 374 cular (axisymmetric) and a rotating elliptic (non-axisymmetric) rigid disks.  
 375 The objective is to compare our formulation with analytical results detailed  
 376 in [Appendix F](#).

377 The systems studied are illustrated in Fig. 3. The inner hollow surfaces  
 378 of the disks are attached with mass-less rigid link to their geometry center  
 379 which coincides with the origin  $O$ . This point is connected to stationary ref-  
 380 erence frame with translational and rotational springs.  $(O; \mathbf{x}, \mathbf{y}, \mathbf{z})$  denotes  
 381 the stationary reference frame, whereas  $(O; \mathbf{x}_r, \mathbf{y}_r, \mathbf{z}_r)$  is a rotating frame

382 attached to the disk. The point  $O$  is also supported with isotropic trans-  
383 lational and rotational bearings of given stiffnesses. The disks are rotating  
384 with a constant spin speed  $\Omega$ .

385 In order to turn the FE model into a rigid model (in other word, to exclude  
386 the effects incoming from flexibility), the Young's modulus of the material  
387 used in the FE model is arbitrarily set extremely high. With respect to the  
388 rigid body hypothesis, no pre-stress is considered. For each disk, the linear  
389 stiffness matrix (calculated with the appropriate boundary conditions and  
390 a very high Young's modulus) at the initial configuration of the model is  
391 directly applied in the modal analysis.

392 A convergence analysis is performed for the rotating circular and elliptic  
393 rigid disks under different spin-speeds. Fig. 4 illustrates the normalized ratio  
394 between the natural frequency obtained via the proposed model and the one  
395 from analytical solution, see [Appendix F](#), as a function of the number of  
396 elements, for different modes and different spin speeds in both circular and  
397 elliptic cases.

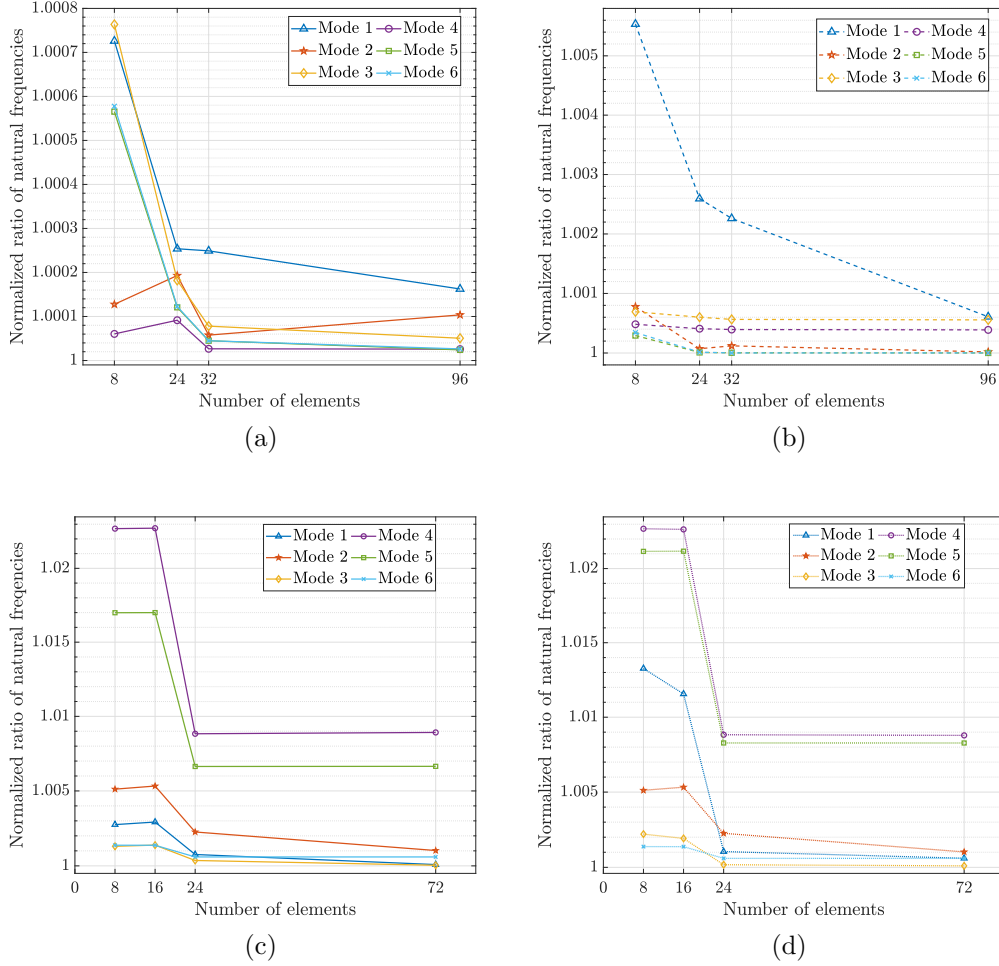


Figure 4: Convergence analysis on the natural frequencies of the first 6 modes of a circular disk ((a) and (b)) and an elliptic disk ((c) and (d)) as a function of the number of elements and for different rotating speeds ((a) and (c):  $\Omega = 10000 \text{ rad/s}$ , (b) and (d):  $\Omega = 20000 \text{ rad/s}$ )

398 The evolution of the natural frequencies of the six rigid body motion  
 399 modes as a function of the spin speed are next compared between the pro-  
 400 posed FE formulation, the conventional FE method [5] and analytical solu-  
 401 tions. The results are illustrated in Fig. 5 for a circular disk and in Fig. 6 for

402 an elliptic disk. These figures show that the frequencies are very well pre-  
 403 dicted by applying the proposed solid FE formulation. On the other hand,  
 404 as the rotational inertia effects play an important role for large values of  
 405 spin speed, the conventional method that neglect these effects is not able to  
 406 predict correctly the three rigid rotational modes (mode 4, 5 and 6) in the  
 407 whole spin speed range.

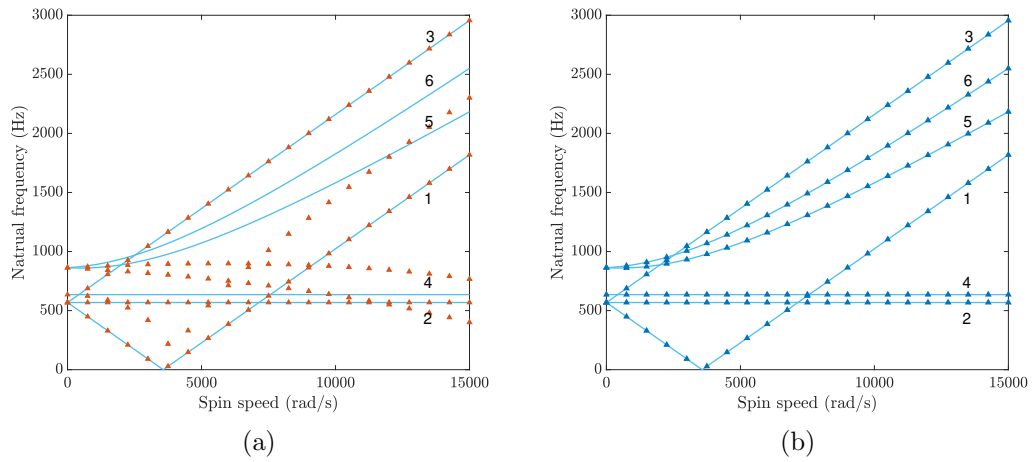


Figure 5: Campbell diagram for a rigid circular disk. Comparison between the analytical solution (-), (a): the conventional method ( $\blacktriangle$ ), and (b): the proposed method ( $\blacktriangle$ )

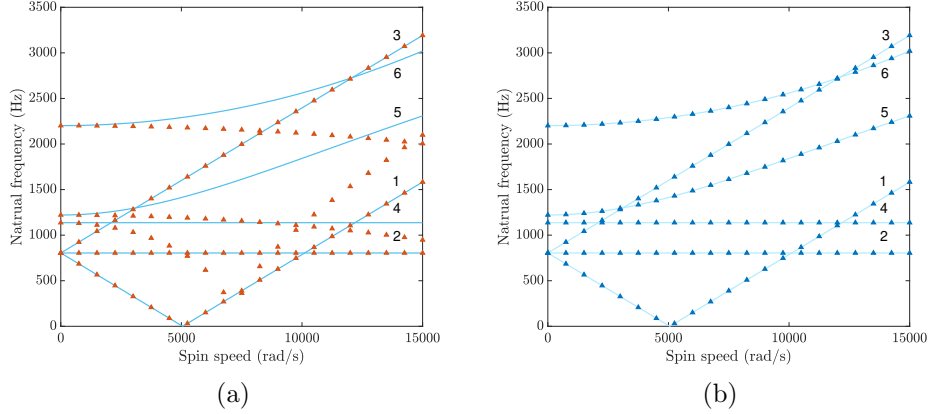


Figure 6: Campbell diagram for a rigid elliptic disk. Comparison between the analytical solution (—), (a): the conventional method ( $\blacktriangle$ ), and (b): the proposed method ( $\blacktriangle$ ).

408        The numerical values used for the simulations are given next. The circular  
 409 disk outer radius  $r_0$  is 0.4 m, whereas the elliptic disk has got a radius on its  
 410 major-axis  $r_a$  of 0.5 m and a radius on its minor-axis  $r_b$  of 0.4 m. Their inner  
 411 radius  $r_i$  and thickness  $h$  are respectively 0.01 m and 0.2 m. Other numerical  
 412 values are: Young's modulus:  $2.1 \times 10^{20}$  Pa; Poisson's ratio 0.3, translational  
 413 bearing stiffness  $K_t$ :  $10^{10}$  N/m, rotational bearing stiffness  $K_r$ ;  $10^{10}$  Nm/rad  
 414 for circular and elliptic cases. The circular and elliptic disks are discretized  
 415 respectively with 96 elements and 72 elements, as illustrated in Fig. 7.

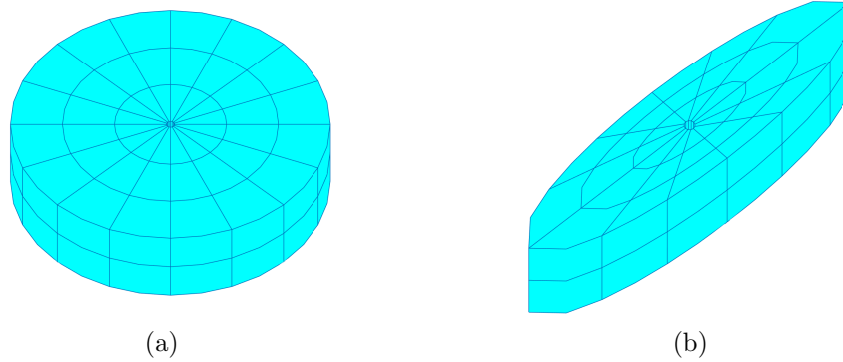


Figure 7: Finite element mesh (a): circular disk with 96 elements, and (b): elliptic disk with 72 elements

416     These two numerical applications validate the proposed enhanced kine-  
 417     matic description in this specific rigid body case. The objective of the next  
 418     application is to validate the whole process, from the consideration of the cen-  
 419     trifugal stiffening to the dynamical analysis around the pre-deformed state.

420     *4.2. Rotating thick beam*

421     In this section, the proposed enhanced solid element is applied to a ro-  
 422     tating flexible beam as the one illustrated in Fig. 8. The beam is clamped  
 423     on one end, and is rotating with a constant spin speed  $\Omega$  around the  $z_r$ -axis.  
 424     The  $y_r$ -axis is chosen to coincide with the centroid axis of the undeformed  
 425     structure, and  $x_r$ -axis and  $z_r$ -axis are chosen to be the principle directions of  
 426     the cross-section. The beam has a uniform rectangular cross-section and is  
 427     made of elastic isotropic material.

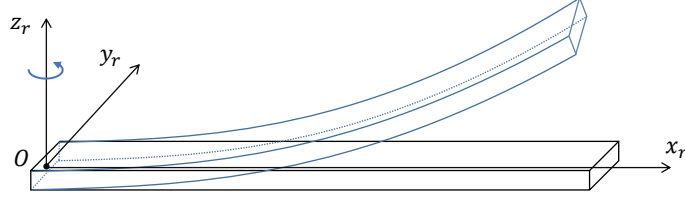
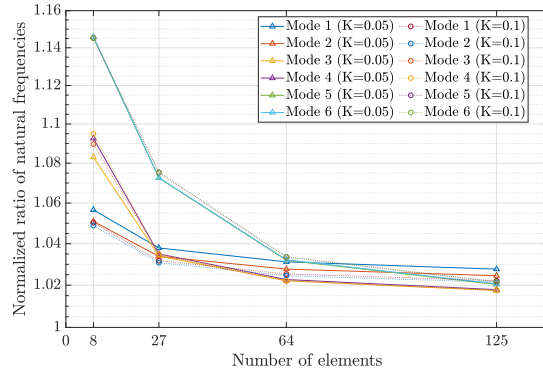


Figure 8: Geometry of a thick rotating Timoshenko beam

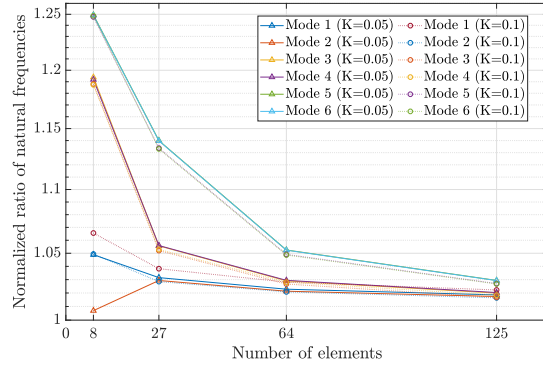
428 The following set of dimensionless parameters will be employed in the  
 429 numerical applications related to this test-case: the dimensionless spin speed  
 430  $K = \Omega L \sqrt{\rho/E}$ , the dimensionless natural frequency  $k = \omega L \sqrt{\rho/E}$  and the  
 431 slenderness ratio  $\eta = 2\sqrt{3}L/h$ , where  $L$  is the length of the beam,  $\rho$  its  
 432 density,  $E$  its Young's modulus,  $h$  the width of the cross-section along the  $z_r$   
 433 direction, and  $\omega$  the natural frequency. To verify the accuracy and versatility  
 434 of the present method, numerical examples obtained for different slenderness  
 435 ratios ( $\eta = 10, 20, 50$ ) are investigated.

436 We first study the convergence of our approach with respect to the number  
 437 of elements in the mesh discretization. Results on the natural frequencies of  
 438 the first 6 lateral modes with different slenderness ratios and different spin  
 439 speeds are compared with analytical reference found in the literature [26]  
 440 based on Timoshenko beam theory. Both centrifugal stiffening effect and  
 441 Coriolis effect are considered. Fig. 9 illustrates the normalized ratio (ratio  
 442 between the natural frequency obtained from the proposed method and the  
 443 analytical one used as reference [26]) as a function of the number of elements,

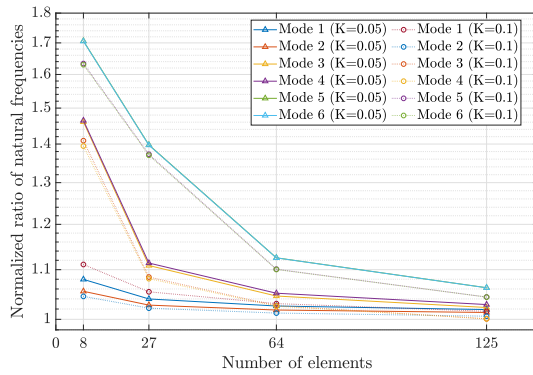
444 for different modes and spin speed.



(a)



(b)



(c)

Figure 9: Ratio between the natural frequencies obtained from the proposed approach and the one from [26], as a function of the number of elements and for different slenderness ratios. (a):  $\eta = 10$ , (b):  $\eta = 20$  and (c):  $\eta = 50$

445 We next compare the natural frequencies of flap-wise and lag-wise modes  
446 of vibration obtained for given values of spin speed ( $K = 0.05$  and  $K = 0.1$ )  
447 between our formulation, the conventional method [5] and reference [26] for  
448 different slenderness ratios ( $\eta = 10, 20, 50$ ). The same number of elements  
449 (125 elements) are used in our formulation and the conventional FE method.  
450 Results are presented in Table 1.

$\eta$	$K$		LW 1	FW 1	LW 2	FW 2	LW 3	FW 3						
10	0.05	A	0.330	2.22%	0.334	2.15%	1.480	1.75%	1.483	1.76%	3.241	2.16%	3.241	2.16%
		B	0.330	2.22%	0.334	2.15%	1.480	1.75%	1.483	1.76%	3.241	2.16%	3.242	2.18%
		Ref.	0.323		0.327		1.455		1.458		3.172		3.173	
	0.1	A	0.332	2.77%	0.347	2.45%	1.486	1.74%	1.497	1.79%	3.252	2.03%	3.256	2.06%
		B	0.330	2.30%	0.346	2.03%	1.487	1.82%	1.498	1.85%	3.257	2.19%	3.261	2.21%
		Ref.	0.323		0.339		1.460		1.471		3.188		3.190	
20	0.05	A	0.176	1.73%	0.183	1.62%	0.982	1.99%	0.984	2.03%	2.414	2.94%	2.415	2.93%
		B	0.176	1.73%	0.183	1.62%	0.982	1.99%	0.984	2.03%	2.415	2.95%	2.415	2.93%
		Ref.	0.173		0.180		0.963		0.965		2.345		2.346	
	0.1	A	0.179	2.01%	0.206	1.64%	0.997	1.68%	1.005	1.84%	2.432	2.70%	2.434	2.67%
		B	0.179	2.01%	0.205	1.47%	1.001	2.01%	1.008	2.15%	2.438	2.95%	2.440	2.91%
		Ref.	0.175		0.203		0.981		0.987		2.368		2.371	
50	0.05	A	0.074	1.89%	0.090	1.33%	0.458	2.30%	0.460	2.88%	1.255	6.25%	1.256	6.25%
		B	0.074	1.89%	0.090	1.33%	0.459	2.52%	0.461	3.10%	1.257	6.44%	1.258	6.43%
		Ref.	0.073		0.089		0.447		0.448		1.181		1.182	
	0.1	A	0.082	1.55%	0.129	0.61%	0.488	0.10%	0.498	0.10%	1.285	4.37%	1.289	4.36%
		B	0.082	1.55%	0.130	0.98%	0.504	2.80%	0.511	2.68%	1.305	6.05%	1.310	6.01%
		Ref.	0.080		0.129		0.487		0.498		1.231		1.235	

Table 1: Dimensionless natural frequencies for lag-wise (LW) and flap-wise (FW) modes of the rotating beam calculated with different approaches (*A*: proposed method, *B*: conventional FE method, based on beam theory [26]) with different slenderness ratios  $\eta$  under dimensionless spin speed  $K$ . The percentage corresponds to the difference between the FE approaches and [26] taken as reference.

451 Table 1 shows that the results found with the proposed formulation are  
452 slightly closer to the solutions based on Timoshenko beam theories than  
453 results generated by conventional FE formulation. However, the differences  
454 between the 2 FE approaches are not substantial in this example. This  
455 is most probably because the effects of rotational inertia included in our

456 model are here almost negligible. The next application deals with this matter  
457 and focuses on a structure in which these effects are expected to be more  
458 important.

459 *4.3. Inclined rotating thick beam*

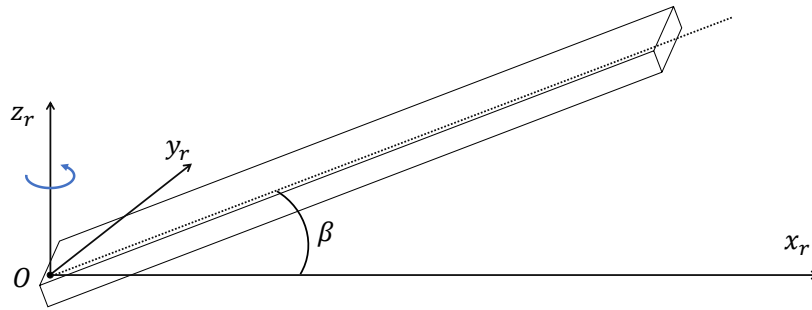


Figure 10: Geometry of a thick rotating inclined Timoshenko beam

460 As our last example, the proposed enhanced solid element is applied to  
461 the inclined rotating beam shown in Fig. 10. The configuration of the beam  
462 is the same as in Fig. 8, except that the axial direction of the beam is inclined  
463 with an angle  $\beta$  in the plane  $(x_r, z_r)$ . When the beam is inclined, the coupling  
464 between centrifugal force and rotational inertia is expected to play a more  
465 important role. Thus, the differences of natural frequencies obtained by the  
466 proposed method and by the conventional method may become more visible.  
467 In the following numerical applications, a moderate thick beam ( $\eta = 20$ ) is  
468 studied as a practical example. We use 64 elements in the simulations. The  
469 inclination angle  $\beta$  may take different values.

$\beta$	K		LW 1	FW 1	LW 2	FW 2	LW 3	FW 3
10°	0.05	A	0.173	0.191	1.009	1.024	2.663	2.679
		B	0.173	0.190	1.010	1.025	2.669	2.683
			-0.14%	0.29%	-0.16%	-0.10%	-0.22%	-0.14%
	0.1	A	0.174	0.214	1.011	1.042	2.636	2.681
		B	0.176	0.212	1.025	1.051	2.685	2.709
			-0.86%	0.92%	-1.33%	-0.87%	-1.81%	-1.00%
20°	0.05	A	0.164	0.198	0.998	1.029	2.647	2.681
		B	0.165	0.197	1.002	1.032	2.661	2.690
			-0.50%	0.37%	-0.43%	-0.29%	-0.53%	-0.53%
	0.1	A	0.159	0.224	0.965	1.041	2.509	2.558
		B	0.165	0.221	1.010	1.061	2.672	2.720
			-3.44%	1.24%	-4.49%	-1.92%	-6.10%	-5.94%
40°	0.05	A	0.148	0.210	0.976	1.036	2.615	2.673
		B	0.150	0.210	0.986	1.044	2.646	2.701
			-1.10%	0.24%	-1.05%	-0.73%	-1.19%	-1.05%
	0.1	A	0.124	0.241	0.855	1.027	2.185	2.270
		B	0.138	0.241	0.978	1.077	2.645	2.739
			-9.94%	0.08%	-12.58%	-4.67%	-17.37%	-17.12%

Table 2: Dimensionless natural frequencies for lag-wise (LW) and flap-wise (FW) modes of the rotating inclined beam calculated with different approaches (*A*: proposed method, *B*: conventional method) with slenderness ratio  $\eta = 20$  under different dimensionless spin speeds  $K$  and inclination angles  $\beta$ .

470 In Table 2, the first 6 flap-wise and leg-wise natural frequencies obtained  
471 with the present method are compared with those obtained by the conven-  
472 tional method [5]. The frequencies obtained by the proposed method are  
473 smaller than the ones simulated by conventional solid elements. The differ-  
474 ence percentage increases with the inclination angle. By considering rota-  
475 tional inertia, the newly proposed spin-softening matrix tends to reduce the  
476 natural frequencies and even more so for an inclined beam. The inclusion  
477 of rotational inertia effects in the formulation corrects the overestimation of  
478 the frequency simulated with the classic solid formulation.

## 479 5. Conclusion

480 This paper presents an extended kinematic description of rotating struc-  
481 tures based on a 3D solid FE formulation that takes rotational inertia effect  
482 into account. The novelty of this formulation lies on the introduction of a  
483 particle-attached reference frame to characterize the rotational orientation.  
484 Furthermore, a general rotation-translation relation is also introduced to ap-  
485 proximate the rotation under small rotation hypothesis.

486 Based on the Total Lagrangian method, a general procedure to evalu-  
487 ate the effect generated by the displacement-dependent centrifugal load was  
488 provided. The centrifugal stiffened pre-deformed state is then used to char-  
489 acterize the new equations of motion. Different numerical applications have  
490 shown that the proposed formulation has great potential in the FE simula-  
491 tion of rotating structures using 3D solid elements. Indeed, as it correctly  
492 accounts for the rotational effects of inertia of the elements, the proposed  
493 approach is appropriate for modeling both rigid and flexible structure at  
494 high spin speed. This will help to accurately predict the vibration behavior  
495 of rotating system. Compared to the conventional FE approach currently  
496 employed in commercial FE softwares, our methodology provides more accu-  
497 rate natural frequencies that are not overestimated from neglected rotational  
498 inertia effects.

499 The formulation was chosen in terms of pure translational degrees of free-  
500 dom in order to be directly compatible with existing FE commercial codes.  
501 It could have been more straightforward to develop an element with both

502 translational and rotational degrees of freedom, but this would be hardly  
503 compatible with existing codes. Therefore, the original proposed FE formu-  
504 lation not only is more accurate to simulate complex rotor dynamics effects  
505 but also has a high potential for industrial implementation.

## 506 **Acknowledgment**

507 The authors would like to acknowledge the financial support of ANSYS-  
508 France.

## 509 **References**

- 510 [1] B. Bediz, L. Romero, O. Ozdoganlar, Three dimensional dynamics of  
511 rotating structures under mixed boundary conditions, *Journal of Sound*  
512 *and Vibration* 358 (2015) 176–191. [doi:10.1016/j.jsv.2015.08.015](https://doi.org/10.1016/j.jsv.2015.08.015).
- 513 [2] Y. J. Kee, S. J. Shin, Structural dynamic modeling for rotating  
514 blades using three dimensional finite elements, *Journal of Mechan-*  
515 *ical Science and Technology* 29 (4) (2015) 1607–1618. [doi:10.1007/  
516 s12206-015-0332-6](https://doi.org/10.1007/s12206-015-0332-6).
- 517 [3] J. Yu, Dynamic analysis of rotor-bearing systems using three-  
518 dimensional solid finite elements, *Psychological Science* 25 (9) (2014)  
519 1682–1690. [doi:10.1007/s13398-014-0173-7.2](https://doi.org/10.1007/s13398-014-0173-7.2).
- 520 [4] C. F. Liu, J. F. Lee, Y. T. Lee, Axisymmetric vibration analysis of  
521 rotating annular plates by a 3d finite element, *International Journal*

- 522 of Solids and Structures 37 (41) (2000) 5813–5827. [doi:10.1016/](https://doi.org/10.1016/s0020-7683(99)00256-5)  
523 [s0020-7683\(99\)00256-5](https://doi.org/10.1016/s0020-7683(99)00256-5).
- 524 [5] G. Genta, Dynamics of rotating systems, Springer, 2005. [doi:10.1007/](https://doi.org/10.1007/0-387-28687-x)  
525 [0-387-28687-x](https://doi.org/10.1007/0-387-28687-x).
- 526 [6] M. Geradin, N. Kill, A new approach to finite element modelling of  
527 flexible rotors, Engineering Computations 1 (1) (1984) 52–64. [doi:](https://doi.org/10.1108/eb023560)  
528 [10.1108/eb023560](https://doi.org/10.1108/eb023560).
- 529 [7] D. Kumar, Rotordynamic analysis using 3d elements in fixed and rotat-  
530 ing reference frame, in: Volume 1: Advances in Aerospace Technology,  
531 ASME, 2016. [doi:10.1115/imece2016-67043](https://doi.org/10.1115/imece2016-67043).
- 532 [8] Z. Shen, B. Chouvion, F. Thouverez, A. Beley, J.-D. Beley, Nonlinear vi-  
533 bration of rotating co-rotational 2d beams with large displacement, Jour-  
534 nal of Engineering for Gas Turbines and Power 141 (5) (2018) 051008–1.  
535 [doi:10.1115/1.4041024](https://doi.org/10.1115/1.4041024).
- 536 [9] S. H. Hashemi, S. Farhadi, S. Carra, Free vibration analysis of rotating  
537 thick plates, Journal of Sound and Vibration 323 (2008) 366–384. [doi:](https://doi.org/10.1016/j.jsv.2008.12.007)  
538 <https://doi.org/10.1016/j.jsv.2008.12.007>.
- 539 [10] ANSYS, ANSYS APDL mechanical theory reference (Oct. 2012).
- 540 [11] D. Kumar, MSC Nastran 2018: rotordynamics user’s guide, MSC Soft-  
541 ware (2018).

- 542 [12] M. I. Friswell, J. E. T. Penny, S. D. Garvey, A. W. Lees, Dynamics of  
543 rotating machines, Cambridge University Press, 2009. [doi:10.1017/  
544 cbo9780511780509](https://doi.org/10.1017/cbo9780511780509).
- 545 [13] R. W. Ogden, Non-linear Elastic Deformations, Dover Publications,  
546 1997.
- 547 [14] N. H. Kim, Introduction to nonlinear finite element analysis, Springer,  
548 2018. [doi:10.1007/978-1-4419-1746-1](https://doi.org/10.1007/978-1-4419-1746-1).
- 549 [15] G. T. Mase, R. E. Smelser, G. E. Mase, Continuum mechanics for engi-  
550 neers, CRC Press, 2010.
- 551 [16] M. Filippi, E. Carrera, Dynamic analyses of axisymmetric rotors through  
552 three-dimensional approaches and high-fidelity beam theories, Journal  
553 of Vibration and Acoustics, Transactions of the ASME 139 (6) (2017)  
554 1–7. [doi:10.1115/1.4036927](https://doi.org/10.1115/1.4036927).
- 555 [17] M. I. Friswell, J. E. T. Penny, S. D. Garvey, A. W. Lees, Dynamics of  
556 rotating machines, Cambridge University Press, 2009. [doi:10.1017/  
557 cbo9780511780509](https://doi.org/10.1017/cbo9780511780509).
- 558 [18] A. Vollan, L. Komzsis, Computational techniques of rotor dynamics  
559 with the finite element method, CRC Press, 2017. [doi:10.1201/b11765](https://doi.org/10.1201/b11765).
- 560 [19] R. B. Borst, M. A. Crisfield, J. C. Remmers, C. V. Verhoosel, Nonlinear  
561 finite element analysis of solids and structures, Wiley, 2012.

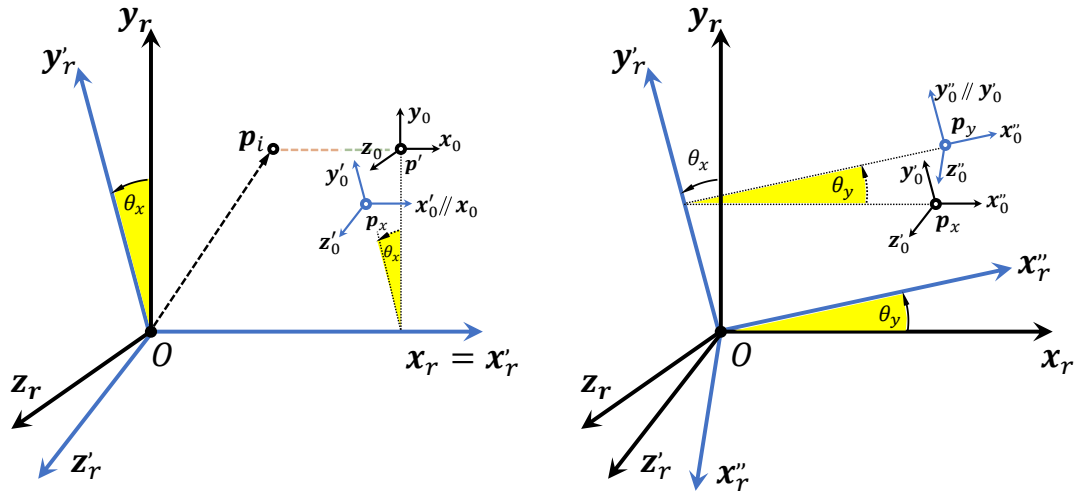
- 562 [20] G. Dhondt, The finite element method for three-dimensional thermo-  
563 mechanical applications, John Wiley & Sons, 2004. [doi:10.1002/  
564 0470021217](https://doi.org/10.1002/0470021217).
- 565 [21] T. Belytschko, W. K. Liu, B. Moran, K. Elkhodary, Nonlinear finite  
566 elements for continua and structures, John wiley & sons, 2013. [doi:  
567 10.5860/choice.38-3926](https://doi.org/10.5860/choice.38-3926).
- 568 [22] N. H. Kim, Introduction to nonlinear finite element analysis, Springer,  
569 2018. [doi:10.1007/978-1-4419-1746-1](https://doi.org/10.1007/978-1-4419-1746-1).
- 570 [23] Z. Sindel, S. Tezcan, Tangent stiffness properties of finite elements,  
571 Computers & Structures 58 (2) (1996) 351–365. [doi:10.1016/  
572 0045-7949\(95\)00130-9](https://doi.org/10.1016/0045-7949(95)00130-9).
- 573 [24] K. J. Bathe, Finite element procedures, Klaus-Jurgen Bathe, 2016.
- 574 [25] J. C. Simo, M. S. Rifai, A class of mixed assumed strain methods and  
575 the method of incompatible modes, International Journal for Numerical  
576 Methods in Engineering 29 (8) (1990) 1595–1638. [doi:10.1002/nme.  
577 1620290802](https://doi.org/10.1002/nme.1620290802).
- 578 [26] S. C. Lin, K. M. Hsiao, Vibration analysis of a rotating timoshenko  
579 beam, Journal of Sound and Vibration 240 (2) (2001) 303–322. [doi:  
580 10.1006/jsvi.2000.3234](https://doi.org/10.1006/jsvi.2000.3234).
- 581 [27] O. D. Ernesto, 3D Motion of Rigid Bodies, Springer International Pub-  
582 lishing, 2019. [doi:10.1007/978-3-030-04275-2](https://doi.org/10.1007/978-3-030-04275-2).

- 583 [28] K. S. Surana, Geometrically nonlinear formulation for the curved shell  
584 elements, *International Journal for Numerical Methods in Engineering*  
585 19 (4) (1983) 581–615. [doi:10.1002/nme.1620190409](https://doi.org/10.1002/nme.1620190409).
- 586 [29] D. N. Bates, The mechanics of thin walled structures with special refer-  
587 ence to finite rotations, Ph.D. thesis, Imperial College (1987).
- 588 [30] O. Gonzalez, A. W. Stuart, *A first course in continuum mechanics*, Cam-  
589 bridge University Press, 2008. [doi:10.1017/cbo9780511619571](https://doi.org/10.1017/cbo9780511619571).

590 **Appendix A. Nomenclature**

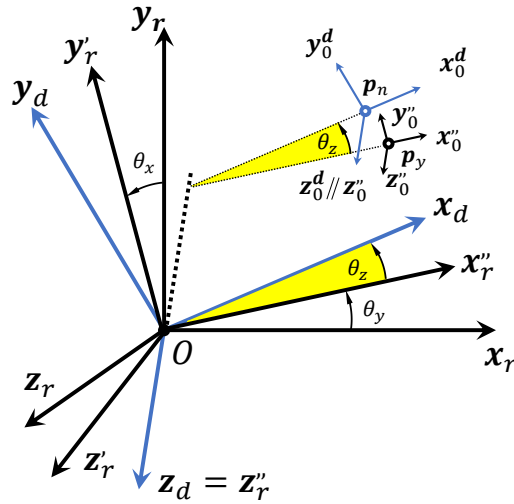
$(O; \mathbf{x}, \mathbf{y}, \mathbf{z})$	stationary reference frame (SRF)
$(O; \mathbf{x}_r, \mathbf{y}_r, \mathbf{z}_r)$	rotating reference frame (RRF)
$(O; \mathbf{x}_d, \mathbf{y}_d, \mathbf{z}_d)$	dynamic reference frame (DRF)
$\theta_x, \theta_y$ and $\theta_z$	classic Euler rotation angles
$(\ )_s, (\ )_r$ and $(\ )_d$	vector expressed respectively in SRF, RRF and DRF
$\mathbf{x}_0, \mathbf{x}_0^d$	initial position expressed respectively in RRF and DRF
$\mathbf{u}$	general translation in RRF
$\tilde{\mathbf{u}}$	second-order approximated rotation-included translation in RRF
$\mathbf{u}_r, \mathbf{u}_d$	elastic translation expressed respectively in RRF and DRF
$\tilde{\mathbf{x}}_r$	second-order approximated position in RRF
$\tilde{\mathbf{x}}_d$	first-order approximated position in DRF
$r_o$ and $r_i$	circular disk outer and inner radius
$r_a$ and $r_b$	radius on its major-axis and minor-axis
$E$	Young's modulus
$L$	length of beam
$h$	thickness of beam
$\rho$	mass density
$\beta$	inclination angle
$\omega$	natural frequency
$\Omega$	global spin speed
$k = \omega L \sqrt{\rho/E}$	dimensionless natural frequency

$K = \Omega L \sqrt{\rho/E}$	dimensionless spin speed
$\eta = 2\sqrt{2}L/h$	dimensionless slenderness ratio
$K_r, K_t$	translational and rotational stiffness of bearing
$\rho_0$	initial mass density
$\varphi_i$	shape function of $i$ -th node in element
$\mathbf{N}$	vector of elemental shape functions
$\mathbf{N}_x, \mathbf{N}_y$ and $\mathbf{N}_z$	spatial derivative of $\mathbf{N}$ along respectively $x$ -, $y$ - and $z$ -direction
$J$	change of volume
${}^0V$	undeformed volume
${}^nV$	current deformed volume
$\mathbf{R}_{u_r}$	translational associated rotational operator
$\mathbf{H}$	rotation matrix with spin speed $\Omega$
$\mathbf{T}$	transformation matrix from SRF to DRF
$\mathbf{D}$	transformation matrix of Euler angles
$\mathbf{e}$	Green-Lagrange strain vector
$\mathbf{C}$	constitutive matrix of material
$\Pi_v$ and $\Pi_s$	kinetic and strain energies
$\Pi_v^{quad}$	quadratic kinetic energy
$\Pi_0^v, \Pi_1^v, \Pi_2^v$ and $\Pi_3^v$	relative, coupling, spin softening and centrifugal kinetic energies
$\mathbf{f}_s$ and $\mathbf{f}_\Omega$	internal elastic force and centrifugal force
$\mathbf{M}, \mathbf{G}, \mathbf{K}_s$ and $\mathbf{K}_\Omega$	mass, gyroscopic, centrifugal stiffening and spin-softening matrices
$\mathbf{K}_\Omega^{core}$	core spin-softening matrix



(a) Rigid rotation  $\theta_x$

(b) Rigid rotation  $\theta_y$



(c) Rigid rotation  $\theta_z$

Figure B.11: Euler angles

592 The Euler angles (which are also referred as Cardan or Bryant angles [27])  
593 are adopted to parameterize the angular orientation  $\mathbf{R}$  of the particle in  
594 Eq. (4). It is assumed that the orthogonal rotation matrix  $\mathbf{R}(\theta_x, \theta_y, \theta_z)$  results  
595 from three successive infinitesimal rotations: firstly, a rotation  $\theta_x$  about the  
596  $\mathbf{x}_r$ -axis (see Fig. B.11a); secondly, a rotation  $\theta_y$  about the new  $\mathbf{y}_r$ -axis (see  
597 Fig. B.11b); and finally a  $\theta_z$  rotation about the new  $\mathbf{z}_d$ -axis (see Fig. B.11c).  
598 The components of the  $[3 \times 3]$  transformation matrix  $\mathbf{R}$  are:

$$\begin{aligned}
\mathbf{R}_{11} &= \cos \theta_y \cos \theta_z \\
\mathbf{R}_{12} &= \sin \theta_x \sin \theta_y \cos \theta_z - \cos \theta_x \sin \theta_z \\
\mathbf{R}_{13} &= \cos \theta_x \sin \theta_y \cos \theta_z + \sin \theta_x \sin \theta_z \\
\mathbf{R}_{21} &= \cos \theta_y \sin \theta_z \\
\mathbf{R}_{22} &= \sin \theta_x \sin \theta_y \sin \theta_z + \cos \theta_x \cos \theta_z \\
\mathbf{R}_{23} &= \cos \theta_x \sin \theta_y \sin \theta_z - \sin \theta_x \cos \theta_z \\
\mathbf{R}_{31} &= -\sin \theta_y \\
\mathbf{R}_{32} &= \cos \theta_y \sin \theta_x \\
\mathbf{R}_{33} &= \cos \theta_x \cos \theta_y
\end{aligned} \tag{B.1}$$

599 It can be easily verified that the final Euler-rotation matrix depends on the  
600 sequence with which the different rotations were applied. A good example of  
601 the issues concerning Euler angles is provided in [28, 29] where it is shown  
602 that the finite element model which uses Euler angles is not always inde-  
603 pendent of this sequence. Thus, in order to get rid of the influence of the

604 lack of uniqueness of Euler angles, the approximation with higher precision  
605 proposed in [29, 18] is applied in this paper. The derivation process of this  
606 approximation is provided next.

607 The second-order approximation begins with the Rodrigues' rotation for-  
608 mula [29]. Based on the small rotation hypothesis, we can define  $\theta$  the  
609 magnitude of the rotation as  $\theta = \sqrt{\theta_x^2 + \theta_y^2 + \theta_z^2}$ , and the corresponding nor-  
610 malized cross-product matrix (skew-symmetric rotation tensor) can be given  
611 by:

$$[\boldsymbol{\omega}] = \begin{bmatrix} 0 & -\theta_z & \theta_y \\ \theta_z & 0 & -\theta_x \\ -\theta_y & \theta_x & 0 \end{bmatrix} \quad (\text{B.2})$$

612 Subsequently, the rotation matrix  $\mathbf{R}$  can be alternatively given by:

$$\mathbf{R} = \mathbf{I} + \frac{\sin \theta}{\theta} [\boldsymbol{\omega}] + \frac{(1 - \cos \theta)}{\theta^2} [\boldsymbol{\omega}]^2 \quad (\text{B.3})$$

613 Substituting  $\sin \theta = \theta$  and  $\cos \theta = 1 - \theta^2/2$  gives the following second-order  
614 approximation of  $\mathbf{R}$ , called  $\tilde{\mathbf{R}}$ :

$$\tilde{\mathbf{R}} = \begin{bmatrix} 1 - (\theta_y^2 + \theta_z^2)/2 & -\theta_z + (\theta_x \theta_y)/2 & \theta_y + (\theta_x \theta_z)/2 \\ \theta_z + (\theta_x \theta_y)/2 & 1 - (\theta_x^2 + \theta_z^2)/2 & -\theta_x + (\theta_y \theta_z)/2 \\ -\theta_y + (\theta_x \theta_z)/2 & \theta_x + (\theta_y \theta_z)/2 & 1 - (\theta_x^2 + \theta_y^2)/2 \end{bmatrix} \quad (\text{B.4})$$

615  $\tilde{\mathbf{R}}$  is the same whatever the sequence of Euler angles used.  $\tilde{\mathbf{R}}$  and  $\mathbf{R}$  share  
616 the same eigenvectors, which helps to be consistent in the rotational axis

617 definition [27, 29]. In Section 2.2,  $\tilde{\mathbf{R}}$  will be used in Eq. (16) to lead to an  
618 extended kinematic relation that takes rotational motion into consideration.  
619 Finally, the useful first-order approximation of  $\mathbf{R}$  is given by:

$$\tilde{\mathbf{R}}^{(1)} = \mathbf{I} + [\boldsymbol{\omega}] \quad (\text{B.5})$$

620 **Appendix C. Kinetic energy expression with enhanced kinematics**  
621 **description**

The explicit expressions of the different components of Eq. (8) are detailed next:

$$\mathbf{M}_0 = \begin{bmatrix} 1 & 0 & 0 & 0 & z_0 & -y_0 & 1 & 0 & 0 \\ & 1 & 0 & -z_0 & 0 & x_0 & 0 & 1 & 0 \\ & & 1 & y_0 & -x_0 & 0 & 0 & 0 & 1 \\ & & & y_0^2 + z_0^2 & -x_0 y_0 & -x_0 z_0 & 0 & -z_0 & y_0 \\ & & & & x_0^2 + z_0^2 & -y_0 z_0 & z_0 & 0 & -x_0 \\ & & & & & x_0^2 + y_0^2 & -y_0 & x_0 & 0 \\ & & & & & & 1 & 0 & 0 \\ & & & & & & & 1 & 0 \\ \text{sym.} & & & & & & & & 1 \end{bmatrix} \quad (\text{C.1})$$

$$\mathbf{G}_0 = \begin{bmatrix}
0 & 1 & 0 & -z_0 & 0 & 2x_0 & 0 & 1 & 0 \\
-1 & 0 & 0 & 0 & -z_0 & 2y_0 & -1 & 0 & 0 \\
0 & 0 & 0 & -x_0 & -y_0 & 0 & 0 & 0 & 0 \\
z_0 & 0 & -x_0 & -x_0y_0 & x_0^2/2 - y_0^2/2 + z_0^2 & -3y_0z_0/2 & z_0 & 0 & -x_0 \\
0 & z_0 & -y_0 & x_0^2/2 - y_0^2/2 - z_0^2 & x_0y_0 & 3x_0z_0/2 & 0 & z_0 & -y_0 \\
0 & 0,0 & y_0z_0/2 & -x_0z_0/2 & 0 & 0 & 0 & 0 & 0 \\
0 & 1 & 0 & -z_0 & 0 & 2x_0 & 0 & 1 & 0 \\
-1 & 0 & 0 & 0 & -z_0 & 2y_0 & -1 & 0 & 0 \\
0 & 0 & 0 & -x_0 & -y_0 & 0 & 0 & 0 & 0
\end{bmatrix}$$

(C.2)

$$\mathbf{K}_{0,\Omega} = \begin{bmatrix}
1 & 0 & 0 & 0 & z_0 & 0 & 1 & 0 & 0 \\
& 1 & 0 & -z_0 & 0 & 0 & 0 & 1 & 0 \\
& & 0 & -y_0 & x_0 & 0 & 0 & 0 & 0 \\
& & & z_0^2 - y_0^2 & x_0y_0 & -x_0z_0/2 & 0 & -z_0 & -y_0 \\
& & & & z_0^2 - x_0^2 & -y_0z_0/2 & z_0 & 0 & x_0 \\
& & & & & 0 & 0 & 0 & 0 \\
& & & & & & 1 & 0 & 0 \\
& & & & & & & 1 & 0 \\
\text{sym.} & & & & & & & & 0
\end{bmatrix}$$

(C.3)

$$\mathbf{f}_1 = \begin{bmatrix} -y_0 & x_0 & 0 & -x_0 z_0 & -y_0 z_0 & x_0^2 + y_0^2 & -y_0 & x_0 & 0 \end{bmatrix}^T \quad (\text{C.4})$$

$$\mathbf{f}_2 = \begin{bmatrix} x_0 & y_0 & 0 & -y_0 z_0 & x_0 z_0 & 0 & x_0 & y_0 & 0 \end{bmatrix}^T \quad (\text{C.5})$$

$$E = \frac{1}{2} \Omega^2 (x_0^2 + y_0^2) \quad (\text{C.6})$$

622 **Appendix D. First-order approximation for  $\mathbf{u}_{def}$  and  $\mathbf{c}$**

623 The explicit expression of  $\mathbf{F}$  in Eq. (11) and the first-order expansion of  
 624  $\mathbf{R}$  in Eq. (B.5) are firstly substituted into Eq. (12) to obtain the following  
 625 second-order expansion form:

$$\begin{aligned} \tilde{\mathbf{u}}_{def}^{(2)} &= \left( (\mathbf{I} + [\boldsymbol{\omega}])^T (\mathbf{I} + \nabla [\mathbf{u}]) - \mathbf{I} \right) \mathbf{p}_0 \\ \tilde{\mathbf{c}}^{(2)} &= (\mathbf{I} + [\boldsymbol{\omega}])^T (-\nabla [\mathbf{u}]) \mathbf{p}_0 + (\mathbf{I} + [\boldsymbol{\omega}])^T \mathbf{u} \end{aligned} \quad (\text{D.1})$$

626 Eq. (13) is then obtained by taking the first-order approximation of Eq. (D.1).

627 **Appendix E. Demonstration of relationship between rotational and**  
628 **translational displacements**

629 In order to find a relationship between local rotations and displacements,  
630 the coordinate vector of a particle in the current configuration is firstly pro-  
631 jected into the dynamic reference as:

$$\mathbf{p}_{n,d} = \mathbf{R}^T (\mathbf{p}_0 + \mathbf{u}) \quad (\text{E.1})$$

632 Since the elastic rotational and translational displacements of  $\mathbf{p}$  are supposed  
633 infinitesimally small,  $\mathbf{p}_{n,d}$  is then first-order approximated as:

$$\tilde{\mathbf{p}}_{n,d} = \begin{bmatrix} x_0 + u_r + \theta_z y_0 - \theta_y z_0 \\ y_0 + v_r - \theta_z x_0 + \theta_x z_0 \\ z_0 + w_r + \theta_y x_0 - \theta_x y_0 \end{bmatrix} \quad (\text{E.2})$$

634 At the same time,  $\mathbf{p}_n$  can also be directly first-order approximated with the  
635 rotational operator  $\mathbf{R}_{\mathbf{u}_r}$  associated with the given translational displacement  
636 field as:

$$\tilde{\mathbf{p}}_{n,d} = \mathbf{u}_r + \mathbf{R}_{\mathbf{u}_r}^T \mathbf{x}_r \quad (\text{E.3})$$

637 where  $\mathbf{x}_r$  is the initial position of the particle expressed in the rotating ref-  
638 erence frame and  $\mathbf{R}_{\mathbf{u}_r}$  is the linearized rotational motion operator defined  
639 with [30]:

$$\mathbf{R}_{\mathbf{u}_r} = \mathbf{I} + \frac{1}{2} \left( [\nabla \mathbf{u}] - [\nabla \mathbf{u}]^T \right) + O(\epsilon^2) \quad (\text{E.4})$$

640  $\nabla$  is the gradient operator with respect to the equilibrium configuration and  
641  $\epsilon = \det(\nabla \mathbf{u})$ . Finally, by equating Eq. (E.2) and Eq. (E.3), the consistent  
642 approximation of elastic rotations can be given as a function of the elastic  
643 translations:

$$\begin{aligned}\theta_x(\mathbf{x}_0) &= \frac{1}{2} \left( \frac{\partial w_r}{\partial y_0} - \frac{\partial v_r}{\partial z_0} \right) \\ \theta_y(\mathbf{x}_0) &= \frac{1}{2} \left( \frac{\partial u_r}{\partial z_0} - \frac{\partial w_r}{\partial x_0} \right) \\ \theta_z(\mathbf{x}_0) &= \frac{1}{2} \left( \frac{\partial v_r}{\partial x_0} - \frac{\partial u_r}{\partial y_0} \right)\end{aligned}\tag{E.5}$$

644 **Appendix F. Analytical equations of motion of a rotating rigid**  
645 **disk**

The governing equations of motion derived in the rotating reference frame for a general rigid disk can be found, for instance, in [12, 18]. The free translational and rotational motions of the disk are decoupled and are governed by:

$$\mathbf{M}_u \ddot{\mathbf{u}}_r + \mathbf{G}_u \dot{\mathbf{u}}_r + \mathbf{K}_u \mathbf{u}_r = \mathbf{0}\tag{F.1}$$

$$\mathbf{M}_\theta \ddot{\boldsymbol{\theta}}_r + \mathbf{G}_\theta \dot{\boldsymbol{\theta}}_r + \mathbf{K}_\theta \boldsymbol{\theta}_r = \mathbf{0}\tag{F.2}$$

where  $\mathbf{u}_r$  and  $\boldsymbol{\theta}_r$  contain respectively the translational and rotational degrees of freedom expressed in the rotating reference frame. The characteristic

matrices of these equations are:

$$\mathbf{M}_u = \begin{bmatrix} m & 0 & 0 \\ 0 & m & 0 \\ 0 & 0 & m \end{bmatrix}, \quad \mathbf{G}_u = \begin{bmatrix} 0 & -2\Omega m & 0 \\ 2\Omega m & 0 & 0 \\ 0 & 0 & 0 \end{bmatrix}$$

and  $\mathbf{K}_u = \begin{bmatrix} K_t - \Omega^2 m & 0 & 0 \\ 0 & K_t - \Omega^2 m & 0 \\ 0 & 0 & K_t \end{bmatrix}$  (F.3)

$$\mathbf{M}_\theta = \begin{bmatrix} I_{xx} & 0 & 0 \\ 0 & I_{yy} & 0 \\ 0 & 0 & I_{zz} \end{bmatrix}, \quad \mathbf{G}_\theta = \begin{bmatrix} 0 & -\Omega(I_{xx} + I_{yy} - I_{zz}) & 0 \\ \Omega(I_{xx} + I_{yy} - I_{zz}) & 0 & 0 \\ 0 & 0 & 0 \end{bmatrix}$$

and  $\mathbf{K}_\theta = \begin{bmatrix} K_r - \Omega^2(I_{yy} - I_{zz}) & 0 & 0 \\ 0 & K_r - \Omega^2(I_{yy} - I_{zz}) & 0 \\ 0 & 0 & K_r \end{bmatrix}$  (F.4)

646  $m$  is the mass of the disk,  $I_{xx}$ ,  $I_{yy}$  and  $I_{zz}$  are its three moments of inertia  
 647 along the three principal axes (which are here chosen to coincide with the  
 648 three axes of the rotating reference frame).  $K_r$  and  $K_t$  are respectively the  
 649 rotational and translational stiffnesses constraining the disk. The natural  
 650 frequencies used as reference in Section 4.1 are the solutions of Eqs. (F.1)  
 651 and (F.2).